International Journal of Heat and Mass Transfer 231 (2024) 125804

Contents lists available at ScienceDirect

International Journal of Heat and Mass Transfer

journal homepage: www.elsevier.com/locate/ijhmt

Enhanced heat transfer correlation for nucleate boiling of fluid mixtures

Zlatan Arnautovic *, Matthias Welzl, Florian Heberle, Dieter Brüggemann

Engineering Thermodynamics and Transport Processes (LTTT), Center of Energy Technology (ZET), University of Bayreuth, Universitätsstraße 30, 95440 Bayreuth, Germany

ARTICLE INFO

Keywords:
Heat transfer
Nucleate boiling
Fluid mixture
Correlations

ABSTRACT

To replace state-of-the-art working fluids in thermodynamic cycles in respect to environmental and efficiency perspective is a current engineering task. In this context, fluid mixtures represent an important research approach. However, the existing correlations for heat transfer coefficient for mixture boiling are complex and uncertain due to diverse thermophysical properties.

In this study, nucleate boiling heat transfer coefficients were experimentally determined for the binary mixtures ethanol/water and ethanol/MM on a vertical falling film at a copper tube for 1 bar and a heat flux range of 40 to 100 kW/m^2. The heat transfer measurements for ethanol/water show a well-known behavior, and coefficients decrease below the pure fluid heat transfer coefficients due to mass transfer resistances. In contrast, measurement data for the ethanol/MM mixture has shown an increase in heat transfer coefficients compared to the pure fluids. The Marangoni effect may have caused this increase. An enhanced heat transfer correlation was proposed based on the correlation of Schlünder under consideration of surface tension and density differences of the pure components. This newly developed correlation is able to predict the heat transfer characteristics of ethanol/water and ethanol/MM very well, and the deviation in the calculation is reduced significantly. The average mean deviation for ethanol/water was 13.3 % and for ethanol/MM only 11.1 %. The general validity of the developed correlation was determined based on ten additional binary mixtures from literature in a pressure range of 1–6 bar and in a heat flux range of 30–1000 kW/m^2. The overall mean deviation concerning the entire data set for the binary mixtures was 18.5 % for Fujita and Tsutsui, 20 % for Inoue and Monde, 18.6 % for the Thome and Shakir correlation, 16.1 % for Schlünder, and 11.6 % for the enhanced correlation.

1. Introduction

The use of mixtures and in particular zeotropic mixtures as working fluids in thermodynamic cycles like Organic Rankine Cycles (ORC), absorption or compression heat pump increases constantly [1–4]. Zeotropic mixtures can lead to a good temperature glide matching in the condenser and the evaporator. In this case, exergy losses are reduced and a higher cycle performance results. Moreover, legislation such as the European Union F-Gas regulation [5], Montreal and the Kyoto Protocol have led to increased application of mixtures. According to the Montreal and the Kyoto Protocol, fluids with an Ozone Depletion Potential (ODP) higher than 0 are forbidden and should also have a Global Warming Potential (GWP) as low as possible. In this context, mixtures are used as substitutes, e.g., R454B (a mixture of R32 and R1234yf as substitute for R410A). Furthermore, potential refrigerants should not be flammable, explosive, toxic or corrosive. These requirements and the recent phase down of fluorinated hydrocarbons reinforce this development [6].

Next to system performance and legal aspects, heat transfer characteristics have to be considered in fluid selection. According to Bai et al. [7], Modi and Haglind [8], Aricapa et al. [9], Wang et al. [10] and Weith et al. [11] zeotropic mixtures improve the overall efficiency of a system. For example, Weith et al. [11] examined the mixture hexamethyldisiloxane (MM)/octamethyltrisiloxane (MDM) for a combined heat and power generation. The authors show that the efficiency could be increased by up to 3 % compared to the most efficient pure fluid for the examined ORC system. Aricapa et al. [9] examined refrigerant mixtures such as R134a, R404A and R410A in their study for refrigeration and air conditioning applications. It was shown that the use of mixtures such as R134a/R1234yf could reduce the GWP by up to 50 % compared to pure R134a. Furthermore, the use of mixtures such as R447A (R32/R1234ze(E)/R125) or R459A (R32/R1234ze(E)/1234yf(E)) showed that a lower GWP of up to 78 % could be achieved compared to R410A and at the same time the COP could be increased by up to 4 %. Wang et al. [10] examined the influence of the siloxane mixture MM/MDM on the net power and efficiency of an ORC compared to the pure substances. They

* Corresponding author.
E-mail address: LTTT@Uni-Bayreuth.de (Z. Arnautovic).

https://doi.org/10.1016/j.ijheatmasstransfer.2024.125804
Received 9 February 2024; Received in revised form 17 April 2024; Accepted 30 May 2024
Available online 14 June 2024

Nomenclature

Latin letters

B_0	coefficient in Eq. (18) (-)
c_p	specific heat capacity (J/kgK)
C_F	coefficient in Eq. (16) (-)
C_{sf}	coefficient in Eq. (8) (-)
d_{MAP}	mean absolute percentate deviation (-)
D	diameter (m)
d_b	bubble diameter (m)
F_r, F_d, F_w	coefficient (-)
g	acceleration due to gravity (m/s^2)
g^E	excess of free enthalpy g (J)
h	heat transfer coefficient (W/m^{2}K)
h	latent heat of vaporization (J/kg)
k	coefficient (-)
k	thermal conductivity (W/mK)
k	coverage factor (-)
L	length (m)
m	coefficient in Eq. (8) (-)
m	coefficient in Eq. (26) (-)
$\widetilde{M}$	molar mass Eq. (16) (kg/mol)
n	coefficient in Eq. (8) (-)
P	electrical evaporator power (W)
p	pressure (bar)
p^*	reduced pressure (-)
Q	heat (W)
$\dot{q}$	heat flux (W/m^2)
R	arithmetic mean roughness height (μm)
r	bubble radius (m)
T	temperature (K)
U	measurement uncertainty in Eq. (4) (-)
u	standard measurement uncertainty (-)
v	mass composition vapor phase (-)
w	mass composition liquid phase (-)
x	mol composition liquid phase (-)
y	mol composition vapor phase (-)

Greek letters

β_l	liquid side mass transfer coefficient (m/s)
β_{SA}	contact angle of the bubble (°)
ρ	density (kg/m^3)
σ	surface tension (N/m)
σ	standard deviation (-)
μ	dynamic viscosity (m/s)
$\Delta\vartheta$	superheating of the liquid, (K)

Subscripts

0	normalization value
1,2	component
$a0$	reference Value
B	boiling
c	critical
c	copper
ca	camber
calc	calculated
db	dew and bubble point
el	electrical
exp	experimental
i	inlet
i,j	components
in	inner tube
id	ideal
g	gas
H_2	hydrogen
l	liquid
m	mixture
m	position sensor
map	mean absolute percentage
mix	mixture
nb	nucleate boiling
o	plane phase interface
o	outlet
ow	outer wall
s	saturation
sol	solder
v	vapor phase
w	wall
w, a	outside copper tube
w, in	inner tube + solder

Abbreviations

ATR unit	attenuated total reflection unit
AZP	azeotropic point
Calc	calculated
DLaTGS	deuterated L-alanine-doped triglycine sulfate
EC	enhanced correlation
FT-IR	fourier transform infrared spectroscopy
F/T	Fujita/Tsutsui
GWP	global warming potential
HTC	heat transfer coefficient
I/M	Inoue/Monde
MM	hexamethyldisiloxane
MDM	octamethyltrisiloxane
NRTL	Non-Random-Two-Liquid-Modell
ODP	ozone depletion potential
ORC	organic ranking cycle
REFPROP	Reference Fluid Thermodynamic and Transport Properties Database
S	Schlünder
T/S	Thome/Shakir
UNIFAC	Universal Quasichemical Functional Group Activity Coefficients
UNIQAUC	Universal Quasichemical
VLE	vapor-liquid-equilibrium

conclude that the thermal stability of the siloxanes has a significant effect on the performance of ORCs, and the use of siloxane blends could improve net performance by 8.1 % compared to pure working fluids.

Unfortunately, thermo-economic investigation from [11–13] reveal a tradeoff due to the application of mixtures with different compositions between an increase in power output and increase in heat transfer surfaces. Therefore, for system design and optimization, precise calculation methods for pure fluids and especially for fluid mixtures are required to predict the heat transfer coefficient (HTC). According to Modi and Haglind [8] and Andreasen et al. [14], the selection of the fluid and the boiling process plays a dominant role in geothermal applications using ORC systems. For example, Andreasen et al. [14] achieve a 15 % higher power output for the isobutane/pentane mixture by optimizing the boiling pressure. It has also been shown that the techno-economic performance of zeotropic mixtures results in lower energy costs compared to pure fluids for ORC or waste heat recovery applications [14].

In the past 70 years, many researchers have carried out experimental investigations for nucleate boiling of pure fluids and mixtures. In the

case of nucleate boiling of mixtures, it is known from numerous studies [15–25] that the heat transfer coefficient is reduced compared to the associated pure fluids. Various mechanisms cause this effect. When evaporating mixtures, heat and mass transfer mechanisms are closely coupled and so mass transfer resistance in the mixture leads to deterioration of the HTC according to Gropp and Schlünder [26]. Furthermore, as with the pure fluids, the thermophysical properties of the fluid mixture play a significant role in the boiling of mixtures. The constantly changing thermophysical fluid properties due to changes in concentration leads to a change in the heat and mass transfer coefficient. Xu et al. [27] show that nucleate boiling of pure fluids and mixtures has been extensively studied over the years from many aspects, with the largest and most significant impacts on pool and flow boiling. Next to the already described mass transfer resistance, nucleate boiling of mixtures can also be influenced by the so-called Marangoni effect [28,29]. There are only few studies on mass transfer and Marangoni convection at pool or flow boiling due to the experimental difficulty. Gropp and Schlünder [26] for example, carried out parallel heat and mass transfer coefficient measurements for nucleate boiling for a vertical falling film for the mixture R11/R113. Vertical falling films enable a visual accessibility of the vaporized gas phase for mass transfer investigations. Furthermore, there are several studies addressing fluid dynamics and heat transfer measurements on a vertical or horizontal liquid film. For example, Fujita and Ueda [30,31] investigated HTC and film breakdowns as a function of the Reynolds number for water in a vertical pipe. In general, the existing investigations are focused on pure fluids.

For example, Weise and Scholl [32] analyzed fluid dynamics and heat transfer on a vertical falling film for pure fluids such as cyclohexanol and propylene glycol with high Prandtl numbers (29 to 663). The authors showed that even at very low Reynolds numbers ($Re < 10$), wavy film structures can occur, and that surface tension effects have an influence on the film dynamics as well as on heat transfer. Seara and Pardiñas [33] compared falling films in horizontal tube evaporators with pool boiling evaporators. For refrigerant systems the authors conclude that the falling film design is a good alternative in terms of operating costs, safety, thermodynamic efficiency, refrigerant charge or size. However, special attention must be paid to fluid distribution around the tube to prevent the film from drying out as well as cracking and to avoid deterioration of the HTCs. The authors also point out that there are numerous empirical correlations for falling films in the literature, but the accuracy of the predictions is usually limited to very specific experimental conditions. Fujita and Tsutsui [34] investigated the heat transfer for the refrigerant R11 on a horizontal tube in case of a falling film at film Reynolds numbers between 10 and 2000. They developed a new empirical heat transfer correlation for pure fluids as a function of the Reynolds number. Additionally, the deterioration of the heat transfer when the film collapses was pointed out by the authors. Alhusseini et al. [35] investigated the heat transfer for water and propylene glycol on a vertical falling film. In this context an empirical correlation was developed, which provided satisfying results for the investigated pure fluids. However, the correlation is not applicable for pool boiling or fluid mixtures.

There are only few studies, which have dealt with the detection and influence of the Marangoni effect [28,29] in relation to pool boiling regime of fluid mixtures. Measurements on the critical heat flux of water, ethanol/water and 1-butanol/water by Hu et al. [36] showed that the critical heat flux was 1.5 times higher for ethanol/water and 1.92 times higher for 1-butanol/water than for pure water. The authors assume that a set Marangoni flow for the mixtures had a positive effect on the heat transfer. Optical measurements at the microscopic level by Namura et al. [37] for ethanol/water and 1-butanol/water support this assumption and have shown a thermal and solutal Marangoni flow around a bubble that is formed. The authors clearly indicated that the use of fluids with a positive Marangoni effect [28,29] can significantly improve the heat transfer of fluid mixtures. To what extent the Marangoni effect [28,29] is based on geometric influences could not be answered by the authors at this point.

Therefore, the influences of mass transfer mechanisms and Marangoni effect [28,29] on nucleate boiling heat transfer using fluid mixtures in vertical liquid films is not well known and requires further investigation. Furthermore, it remains unclear how these influences can be considered in nucleate boiling heat transfer correlations for mixtures.

Currently, empirical or semi-empirical correlations can be used to calculate the HTCs, which are only applicable for a limited number of fluids and in a range of operating parameters, such as the well-known correlations of Schlünder [21], Thome and Shakir [38] or Fujita and Tsutsui [18] for fluid mixtures. However, most calculation methods require reliable mixture property data like vapor-liquid equilibrium (VLE), density, surface tension or enthalpy of vaporization. These data are often not available for certain fluids or mixture combinations, or are sometimes very error-prone when calculating with inadequate calculation models. Arnautovic et al. have shown in previews studies [39,40] that depending on the choice of the calculation method, massive uncertainties and errors can occur when calculating VLE data or transport properties of siloxane mixtures.

In this paper, heat transfer coefficients for ethanol/water and a mixture of the linear siloxane MM with ethanol are measured on a vertical copper tube on a falling liquid film. Furthermore, reliable heat transfer correlations for ethanol/water and ethanol/MM should be identified. An extended correlation for nucleate boiling of mixtures is also developed and presented. The proposed correlation can be used with accessible fluid properties and is validated with different liquid mixtures such as zeotropic and azeotropic or different fluid classes.

2. Experimental setup and methodology

The presented experiments include heat transfer measurements of water/ethanol and ethanol/MM mixtures on a vertical tube under falling film conditions. The fluids, the experimental setup, and the data reduction are described in detail in the following sections.

2.1. Investigated fluids

For the experiments, ethanol and distilled water were used with a mass fraction purity of $>$ 99.95 % according to the supplier VWR Chemicals. The purity of the siloxane MM from Wacker Chemie AG is $>$ 99.50 % and was measured by the supplier using gas chromatography (GC). Table 1 lists the specifications of the investigated fluids.

The mixtures, ethanol/water and ethanol/MM are examined in a range of 0 to 100 % in 20 % steps. Studies by Angelino and Paliano [41] and Abbas et al. [42] showed the potential of siloxanes and their mixtures as working fluids in high-temperature ORC processes. Ethanol/-water is a well-known mixture [15,18,21,43] and will be used with the pure fluids for validation with available literature data.

2.2. Experimental setup

To measure the heat transfer coefficient an experimental setup shown in Fig. 1 has been developed.

The pure fluids and mixtures are pumped from the fluid tank into a

Table 1
Information and purity of the components.

Fluid	Chemical formula	CAS number	Molar mass (g/mol)	Purity (mass frac.)	Supplier
Ethanol	C_2H_6O	64–17–5	46.068	$>$ 99.95 %	VWR Chemicals
Water	H_2O	7732–18–5	18.015	$>$ 99.95 %	VWR Chemicals
MM	$C_6H_{18}OSi_2$	107–46–0	162.38	$>$ 99.50 %	Wacker Chemie AG

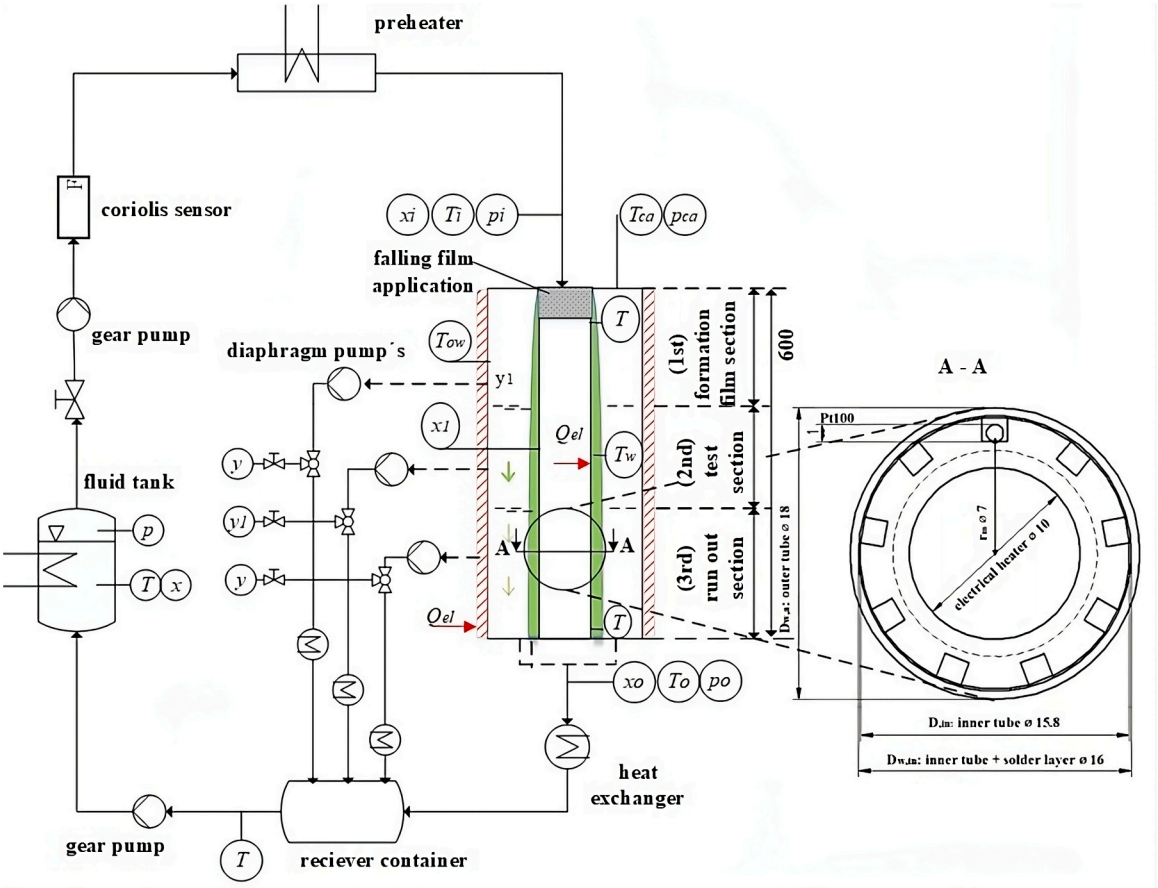

Fig. 1. Schematic diagram of the experimental setup.

preheater section by using a gear pump. The mass flow is measured by a coriolis mass flow sensor. In the preheater, the fluid is heated close to saturation temperature (T_i, x_i) before entering the measurement section. In order to provide a falling film application, the fluid first is led through a porous stainless-steel filter with a length of 50 mm, an outer diameter of 17 mm and a pore size of approximately 40 μm. The falling film flows down an electrically heated vertical copper tube and is partially evaporated. The remaining liquid part is cooled at the outlet of the measurement section by a heat exchanger and then led into a collection container. The vapor part is split off continuously, perpendicularly to the evaporator surface via diaphragm pumps, condensed and also led into the receiver container. This procedure ensures constant pressure in the measurement section. The fluid in the receiver container is pumped back by a gear pump into the fluid tank.

The evaporation tube is located in a stainless-steel chamber, which has six sight glasses for optical analysis of the falling film. It is also electrically heated from the outside to avoid condensation on the inner wall of the chamber (T_{ow}). Liquid samples can be taken at the outlet of the stainless-steel chamber (x_1) and via the diaphragm pumps at each section (y). The cross-section of the evaporator tube is shown in Fig. 1 on the right side and consists of two copper tubes (material CW024A), a heating cartridge with a diameter of 10 mm and soldered temperature sensors to determine the outside wall temperature. The structure of the evaporator tube is adapted from Welzl [44,45] and consists types of components. The evaporator tube is heated over a length of 500 mm by the heating cartridge, which is located in the inner copper tube. Furthermore, grooves are milled on the outside of the inner tube. In total, nine Pt100 sensors are soldered into these grooves and used to measure the temperature on the inside of the outer copper tube. Measuring the temperature on the inside of the outer tube, the wall temperature T_w of the outer tube can be calculated, considering the heat conduction inside the copper tube and the solder. In each case, three sensors were introduced at 120° at the inlet ($l_1 = 400$ mm, 1st section) and outlet ($l_3 = 50$ mm, 3rd section). Hereby, the radial temperature profile can be recorded. Finally, three temperature sensors are installed at a length of $l_2 = 220$ mm (2nd section) to determine the heat transfer coefficients. The 1st section is related to the formation of a hydrodynamic liquid film. The 2nd segment is the actual test section and the third segment represents the run-out section. The vapor is drawn off separately in the respective segments via 4 connections by the respective diaphragm pump to prevent the vapor from flowing parallel to the falling film to avoid further mass transfer resistance.

2.3. Methodology measurement

For pure fluids, the respective saturation temperature can be determined via the measured pressure (p_{ca}). Fluid temperature could not be measured directly, because, the fluid film would be too thin and it would have to be measured directly in the film. This could influence the flow of the fluid film and cause uncertainties.

For the fluid mixtures, the saturation temperature is determined via the pressure measured in the chamber (which is always regulated to 1 bar) and liquid samples which are taken from the falling film in the second section.

In the next step, the local nucleate boiling heat transfer coefficient is defined as:

$$h_{nb} = \frac{\dot{q}}{T_w - T_s(p_{ca},\ x_1)} \tag{1}$$

with h_{nb} for the nucleate boiling HTC and $\dot{q}$ as the heat flux

$$\dot{q} = \frac{P_{el}}{\pi\, D_{w,a}\, L} \tag{2}$$

where P_{el} corresponds to the measured electrical power of the heating cartridge, $D_{w,a}$ represents the outside diameter of the evaporator tube and L is the heated length.

T_w is the outer wall temperature, which can be calculated according to

$$T_w = \frac{1}{3}\sum_{j=1}^{3}\left(T_{in,j} - \dot{Q}\left(\frac{\ln\left(D_{in}/D_{m,j}\right)}{2\,\pi\, L\, k_{c,in}}\right)\right) - \dot{Q}\left(\frac{\ln\left(D_{w,in}/D_{in}\right)}{2\,\pi\, L\, k_{sol}}\right) + \left(\frac{\ln\left(D_{w,a}/D_{w,in}\right)}{2\,\pi\, L\, k_{c,a}}\right) \tag{3}$$

where $T_{in,j}$ is the measured inner temperature of the temperature sensor and $k_{c,in}$ is the thermal conductivity of the inner copper tube, k_{sol} of the soldered material and $k_{c,a}$ of the outer copper tube. The diameters used can be seen in Fig. 1 and represented in Eq. (3), where D_{in} is the inner tube diameter, $D_{w,in}$ the inner tube with solder and $D_{w,a}$ the outer tube diameter. $D_{m,j}$ is the diameter of the measurement position of the temperature sensor. The saturation temperature of the liquid is $T_s(p_{ca},\ x_1)$ and was calculated applying the g^E-model NRTL. Through investigations and previous VLE measurements [39], the NRTL model was identified for a reliable calculation for the saturation temperature for ethanol/-water. The appropriate models for the ethanol/MM can be seen in Fig. 19 in the appendix. Measuring points are recorded in a stationary state and a value is recorded every second for 3 min. Table 2 lists the used main components and its characteristic parameters.

2.4. Sample analysis and uncertainties

The composition of the vapor and liquid samples is analyzed with Fourier transform infrared spectroscopy (FT-IR) using a Bruker Invenio R apparatus with an Attenuated Total Reflection Unit (ATR unit). The ATR covers a spectral range from 0 to 5000 cm^{-1}. The device is equipped with a potassium bromide beam splitter as standard. The integrated helium-neon laser emits red light with a wavelength of 633 nm and a power of 0.8 mW. This serves to position the movable mirror of the interferometer. A highly stable ROCKSOLID interferometer with two cube-shaped retroreflectors is used as the interferometer. Thanks to the high light throughput, the device has a high signal-to-noise ratio. The device contains a deuterated L-alanine-doped triglycine sulfate (DLaTGS) detector as standard and works with a spectral resolution of 0.16 cm^{-1} and a wave number accuracy of 0.005 cm^{-1} [46].

The procedure to determine the standard and maximum deviation of the FT-IR system with the ATR unit, was as follows. The first step was to acquire reference spectra for the mixtures which are examined. For this purpose, samples were prepared and mixed using a precision balance (SARTORIUS CUBIS® semi-micro balance 225P) with a repeatability of 0.04 mg and reading accuracy of 0.01 mg. The respective components are filled one after the other into a sample vessel using a syringe. The fine dosing is carried out using a syringe cannula with a diameter of 0.4 mm. The target weight of a sample is set at 100 g. The error of mixing by the balance is 0.0001 % and can be neglected. The sample with known concentration is sealed and measured with the ATR unit. In total, each sample is measured five times and then an average value is formed from all the measured spectra, which represents the reference spectrum for this concentration. Fig. 2 shows the reference spectra for ethanol/MM. For a better overview, only spectra in a range from 0 to 100 % ethanol are shown in 10 % steps. For the actual evaluation, reference spectra were created in 5 % steps. These measured reference spectra were used to determine the concentration of the liquid samples taken from the experimental setup.

Table 2
Components and accuracy of measurement devices.

Component	Type	Value Range
Gear Pump	Verder VGS200.10	3–6 kg/min
Diaphragm pump	Schwarzer SP 620	4,6 l/min
Coriolis Sensor	TMU-S008	200 kg/h
Temperature Sensor	Pt100 1/3 DIN, B	600 °C
Pressure Sensor	Piezoresistive pressure transducer PAA-3SY, (125 °C)	5 bar

In order to evaluate the measurement uncertainty of this method, samples were mixed again using the precision balance, with different concentrations. Then, new spectra were measured and analyzed for their concentration using the reference spectra and compared to the known concentrations. This procedure was carried out over the entire concentration range (0 – 100 %) with eleven samples, where each sample was measured three times and there was a maximum deviation of the concentration evaluated using the reference spectra of ± 0.5 % and a standard measurement uncertainty of 0.29 % (mass fraction).

The measurement uncertainty for the heat transfer coefficient is determined according to the Guide to the Expression of Uncertainty in Measurement (GUM) [47]. The total amount of measurement uncertainty is about

$$U_h = k\, u_{c,h} \tag{4}$$

shown. Here, k is the coverage factor with a value of 2. Assuming a normal distribution, this value results in a coverage probability of 95 % and $u_{c,h}$ is the defined standard measurement uncertainty and is defined as

$$u_{c,h} = \sqrt{(\sigma_h^2 + u_h^2)} \tag{5}$$

with the standard deviation

$$\sigma_h = \sqrt{\frac{1}{N(N-1)}\sum_{i=1}^{N}(a_i - \bar{a})^2} \tag{6}$$

where N is the number of data, $\bar{a}$ is the mean value of the output variable and a_i are the individual values of the output variable. The standard measurement uncertainty u_h is determined via error propagation

$$u_h = \sqrt{\sum_{i=1}^{m}\left(\frac{\partial h_{nb}}{\partial x_i}\, u_i\right)^2 + \sum_{i=1}^{m-1}\sum_{j=i+1}^{m}\frac{\partial h_{nb}}{\partial x_i}\,\frac{\partial h_{nb}}{\partial x_j}\, u(x_i, x_j)} \tag{7}$$

with the dependent variables. Due to its low influence, the covariance

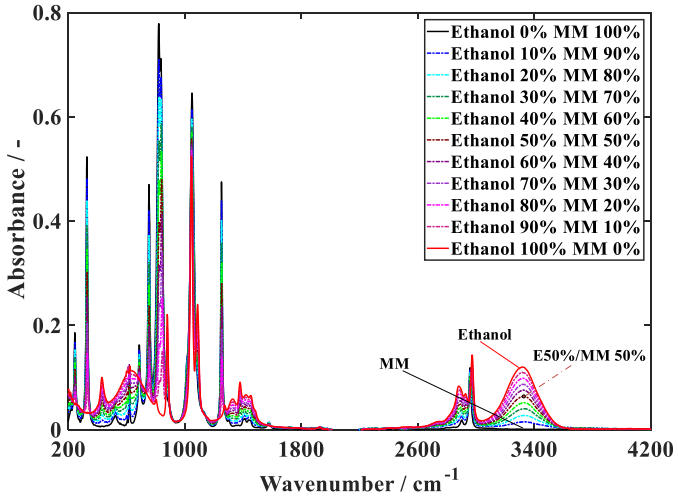

Fig. 2. FT-IR spectra for ethanol/MM mixture at 20 °C, 1 bar and 10 % concentration steps in mass%.

term was no longer considered. The uncertainty contributions are summarized in Table 7 in the appendix.

When determining the deviation of the saturation temperatures, there are various contributions that must be taken into account. The first is the temperature deviation due to the concentration deviation $T_s(x_1)$. The deviation can be stronger or weaker depending on the slope of the VLE curve and was calculated for each individual measuring point. Second is the deviation between the calculated VLE curve according to NRTL and measured VLE points from previous investigations T_s(VLE). Since it was not possible to measure a separate saturation temperature for each heat transfer measuring point, the standard deviation between the measuring points (VLE) and the calculated values from NRTL was used. The third point is the pressure dependence of the VLE curves $T_s(p)$.

3. Nucleate boiling correlations

According to the VDI heat atlas [48], the HTC for nucleate boiling of falling films is independent of the Reynolds number or mass flow, just as it is for pool boiling. This means that the HTC are independent of the alignment of an evaporator surface (horizontal or vertical). Fujita and Ueda [30] investigated nucleate boiling HTC for water on a vertical steel tube using the Nishikawa's correlation [49]. This correlation was originally developed for pool boiling on a horizontal plate, but showed good agreement with the measurement data from Fujita and Ueda [30]. Oliveira et al. [50] investigated nucleate boiling of ethanol on a platinum wire and Shen et al. [51] nucleate boiling of ethanol on a horizontal copper plate. Both works have measured the similar heat transfer coefficients up to a heat flow density of 300 kW/m^2. Furthermore, Gropp and Schlünder [26] showed in their work that the Schlünder correlation [21], which was used for numerous fluid mixtures for nucleate boiling on horizontal tubes or plates, that the calculated HTC provided excellent agreement with Gropp and Schlünder [26] measured data for the mixture R11/R113, which were collected on a vertical falling film. This indicates that the heat transfer coefficient for nucleate boiling is independent of heater orientation and shape, and those common nucleate boiling correlations for pure fluids and mixtures are applicable to a vertical falling film.

In order to identify suitable correlations, existing models are investigated and compared with the experimental data. In addition, an enhanced approach to calculate the heat transfer coefficients for nucleate boiling of the mixtures is also proposed and compared with the measurement data and the other correlations. First correlations for pure fluids are presented and then the correlations for mixtures.

3.1. Pure fluids

The correlations of Rohsenow [52], Stephan and Abdelsalam [53] and Gorenflo [48], were preselected and used for the calculation of the nucleate boiling HTC. The Rohsenow correlation [52] was chosen due to its explicit parameters for copper/ethanol and according to Shen et al. [51], this provides good agreement with the measurement data. The same applies to the correlation of Stephan and Abdelsalam [53] and the modified Gorenflo correlation from the VDI Heat Atlas [48], which have provided good agreement for a various amount of pure fluids, including ethanol and water.

Rohsenow [52] developed a nucleate boiling correlation for various fluids, which can be calculated HTCs as follows

$$\frac{c_p\,(T_w - T_s)}{\Delta h_v} = C_{sf}\left[\frac{\dot{q}}{\mu\,\Delta h_v}\sqrt{\frac{\sigma}{g\,(\rho_l - \rho_g)}}\right]^m \left(\frac{c_p\,\mu}{k_l}\right)^n. \tag{8}$$

Here, c_p is the specific heat capacity, Δh_v the latent heat of vaporization, μ the dynamic viscosity, $\dot{q}$ the heat flux, g is the gravitational acceleration, σ is the surface tension, k_l is the thermal conductivity, and ρ_l and ρ_g are the liquid and vapor densities of the liquid. The parameters C_{sf}, m and n are empirical coefficients and exponents that depend on the evaporator surface and fluid combination. Pioro [54] lists coefficients for numerous surface and fluid combinations.

The correlation of Stephan and Abdelsalam [53] was developed by multiple regression on various measurement data groups and is divided into 4 groups: Water, hydrocarbon (organics), cryogenics and refrigerants. The correlation related to hydrocarbon (organics) is defined as

$$h_{nb} = 0.0546\left(\frac{k_l}{d_b}\right)\left[\left(\frac{\rho_g}{\rho_l}\right)^{1/2}\left(\frac{q\,d_b}{k_l\,T_s}\right)\right]^{0.67}\left(\frac{\rho_l - \rho_g}{\rho_l}\right)^{-4.33}\left(\frac{\Delta h_v\,d_b^2}{\alpha_l^2}\right)^{0.248} \tag{9}$$

with α_l as the thermal diffusivity of the pure fluid and the bubble departure diameter of the pure fluid

$$d_b = 0.0146\,\beta\left[\frac{2\,\sigma}{g\,(\rho_l - \rho_g)}\right] \tag{10}$$

where β is the contact angle between the bubble and the surface.

For nucleate boiling of pure fluids in a vertical downflow tube, Gorenflo [48] proposed the following correlation

$$h_B = h_0\,C_F\left(\frac{\dot{q}}{\dot{q}_0}\right)^n F_r\,F_d\,F_W \tag{11}$$

where α_0 is the normalization value at $p_r = p/p_c = 0.1$. The fluid-specific value $\dot{q}_0$ is determined in ([48], Section H3) by

$$n = 0.8 - 0.1\cdot 10^{(0.76\cdot p_r)}. \tag{12}$$

The influence of the boiling pressure is represented by

$$F_r = 2.816\,p_r{}^{0.45} + \left(3.4 + \frac{1.7}{1 - p_r{}^7}\right)p_r{}^{3.7}. \tag{13}$$

The tube dimensions are taken into account in F_d and can be calculated using the following equation

$$F_d = \left(\frac{d_0}{d}\right)^{0.4} \tag{14}$$

with $d_0 = 10^{-2}$ m and d as the tube diameter. The heating wall properties F_W are

$$F_W = \left(\frac{R_a}{R_{a0}}\right)^{0.133} \tag{15}$$

with $R_{a0} = 1x10^{-6}$ m and for the roughness of the copper R_a is assumed as 0.2 μm according to supplier [55,56].The C_F value takes into account the molar mass $\tilde{M}$ of a fluid and can be determined according to

$$C_F = 0.435\left(\frac{\tilde{M}}{\tilde{M}_{H2}}\right)^{0.27}, \tag{16}$$

where $\tilde{M}_{H2}$ is the molar mass of hydrogen.

3.2. Mixtures

The widely used correlations of Schlünder [21], Thome and Shakir [38], Fujita and Tsutsui [18] and Inoue and Monde [23] are used to calculate the nucleate boiling HTC for the mixtures. They have proven quite resilient to a wide variety of fluids, and have been used on an ethanol/water system by all the mentioned authors. Furthermore, the selected correlations do not require any empirical mixture-dependent parameters.

According to Schlünder [21], the nucleate boiling HTC for mixtures $h_{nb,m}$ can be calculated as follows

$$\frac{h_{nb,m}}{h_{id}} = \left(1 + \frac{h_{id}}{\dot{q}} \sum_{i=1}^{n} \left[\left(T_{S,n} - T_{S,i}\right)\left(y_i - x_i\right) k_l\right]\right)^{-1} \tag{17}$$

with

$$k_l = \left(1 - exp\left(\frac{-B_0\ \dot{q}}{\rho_{l,m}\ \Delta h_{v,m}\ \beta_l}\right)\right). \tag{18}$$

h_{id} is the ideal heat transfer coefficient of the mixture and is defined as

$$h_{id} = \sum_{i=1}^{i=n} \left(\frac{x_i}{h_{i,nb}}\right)^{-1} \tag{19}$$

where x_i and y_i are the mole fraction of the liquid and vapor of the mixture and $h_{i,nb}$ represents the heat transfer coefficient. $T_{S,n}$, $T_{S,i}$ are the saturation temperature of the pure fluids. B_0 is a correction factor that takes into account the proportion of heating power required for nucleate boiling, which is normally set to $B_0 = 1$, $\rho_{l,m}$ is the liquid mixture density and $\Delta h_{v,m}$ is the latent heat of evaporation of the mixture. β_l is the liquid-side mass transfer coefficient, which has a value between $\beta_l = 1.3 - 2 \cdot 10^{-4}$ m/s according to Schlünder [21].

Thome and Shakir [38] proposed a very similar correlation compared to the correlation of Schlünder [21], which is defined as

$$\frac{h_{nb,m}}{h_{id}} = \left(1 + \frac{h_{id}}{\dot{q}} \left[\left(T_{y,i} - T_{x,i}\right) k_l\right]\right)^{-1}. \tag{20}$$

The difference to the Schlünder [21] correlation is that the saturation temperature of the pure fluid is not used, but rather the ratio of the respective boiling point $T_{x,i}$ and the dew point temperature $T_{y,i}$ at the concentration x_i.

Fujita and Tsutsui [18] developed a different approach and propose the following equation to calculate the heat transfer coefficients for mixtures

$$\frac{h_{nb,m}}{h_{id}} = \left(1 + \left[1 - k_j\right] \frac{\left(T_{y,i} - T_{x,i}\right)}{\Delta T_{id}}\right)^{-1} \tag{21}$$

with

$$k_j = \left(exp\left(\frac{-60\ \dot{q}}{\rho_{v,m} \Delta h_{v,m} \left[\sigma_{l,m}\ g\ \left(\rho_{l,m} - \rho_{v,m}\right) \Big/ \rho_{v,m}^2\right]^{1/4}}\right)\right). \tag{22}$$

The exponent k_j includes a greater consideration of the liquid and vapor densities $\rho_{l,m}$ and $\rho_{v,m}$ and ΔT_{id} is the ideal wall superheat in a mixture and can be calculated according to

$$\Delta T_{id} = \frac{\dot{q}}{h_{id}}. \tag{23}$$

An alternative approach was developed by Inoue and Monde [23] and is defined as follows

$$\frac{h_{nb,m}}{h_{id}} = \left(1 + k_i \frac{\left(T_{y,i} - T_{x,i}\right)}{\Delta T_{id}}\right)^{-1} \tag{24}$$

with

$$k_i = 0.45 \cdot 10^{-5} \cdot \dot{q} + 0.25. \tag{25}$$

The approach of Inoue and Monde [23] is different in comparison to the approaches presented before, because no properties of the mixtures, except of the VLE data, are taken into account. Instead empirical constants were used, which were derived from experimental data of the mixtures R12/R113, R134a/R113, R22/R113 and R22/R11.

To sum up chapter 3, the correlations which were used to calculate the heat transfer coefficients are listed in Table 3.

Table 3
Considered correlations for nucleate pool boiling heat transfer coefficients of pure fluids and mixed fluids.

Pure fluid	
Author	Correlation
Rohsenow (1952) [52]	$\frac{c_p\ (T_w - T_s)}{\Delta h_v} = C_{sf} \left[\frac{\dot{q}}{\eta\ \Delta h_v} \sqrt{\frac{\sigma}{g\ (\rho_l - \rho_g)}}\right]^m \left(\frac{c_p\ \eta}{\lambda_l}\right)^n$
Stephan und Abdelsalam (1980) [53]	$\alpha_B = 0,$ $0546 \left(\frac{\lambda_l}{d_b}\right) \left[\left(\frac{\rho_g}{\rho_l}\right)^{1/2} \left(\frac{q\ d_b}{\lambda_l\ T_s}\right)\right]^{0.67} \left(\frac{\rho_l - \rho_g}{\rho_l}\right)^{-4,33} \left(\frac{\Delta h_v\ d_b^2}{\alpha_l^2}\right)^{0,248}$
Gorenflo (1993) [48]	$\alpha_B = \alpha_0\ C_F \left(\frac{\dot{q}}{\dot{q}_0}\right)^n F(p^*)\ F(d)\ F(W)$
Fluid mixture	
Author	Correlation
Schlünder (1982) [21]	$\alpha_{B,m} = \alpha_{id} \left(1 + \frac{\alpha_{id}}{\dot{q}} \sum_{i=1}^{n-1} \left[\left(T_{S,n} - T_{S,i}\right)\left(y_i - x_i\right) k_l\right]\right)^{-1}$ $k_l = \left(1 - exp\left(\frac{-B_0\ \dot{q}}{\rho_{l,m}\ \Delta h_{v,m}\ \beta_l}\right)\right)$
Thome und Shakir (1987) [38]	$\alpha_{B,m} = \alpha_{id} \left(1 + \frac{\alpha_{id}}{\dot{q}} \left[\Delta T_{bp}\ k_l\right]\right)^{-1}$
Inoue und Monde (1994) [23]	$\alpha_{B,m} = \alpha_{id} \left(1 + \frac{\Delta T_{bp}}{\Delta T_{id}} \left[0,45 \cdot 10^{-5}\ \dot{q} + 0,25\right]\right)^{-1}$
Fujita und Tsutsui (1997) [18]	$\alpha_{B,m} = \alpha_{id} \left(1 + \left[1 - k_j\right] \frac{\left(T_{y,i} - T_{x,i}\right)}{\Delta T_{id}}\right)^{-1}$ $k_j = \left(exp\left(\frac{-60\ \dot{q}}{\rho_{g,m}\ \Delta h_{v,m} \left[\sigma_{l,m}\ g\ \left(\rho_{l,m} - \rho_{g,m}\right) / \rho_{g,m}^2\right]^{1/4}}\right)\right)$

4. Development of an enhanced heat transfer correlation

For the correlations concerning nucleate boiling of pure fluids, it was already discussed that the correlations lead to low uncertainties compared to measurement data for a high variety of pure fluids, which can be seen in chapter 3 in the publications by Rohsenow [52], Stephan and Abdelsalam [53], Gorenflo [48] or Pioro [54]. In addition, the availability and reliability of fluid properties is given in case of pure fluids. Therefore, there is less need to adjust and improve existing models for the pure fluids.

Far greater challenges arise when estimating the heat transfer coefficient of mixtures at nucleate boiling. While for nearly ideal mixtures, with components of the same fluid class, a reduction of the heat transfer can estimate well, this is not the case for non-ideal mixtures. The reasons for this include the reliability and accessibility of the fluid data and the scope of the corresponding measurement campaigns. This relationship is illustrated in Fig. 3.

Furthermore, all the correlations, except for Fujita and Tsutsui [18], do not consider the surface tension, which has a major influence on the heat transfer, as mentioned in chapter 3. Thus, it can be seen that the correlations can all well prediction decreasing, but not increasing heat transfer coefficients, which can be caused by the Marangoni effect [28, 29], as shown in the measurement data of Gropp and Schlünder [26] and Sakai et al. [57] in Fig. 3.

Here, the well-known correlations of Schlünder [21], Thome and Shakir [38], Fujita and Tsutsui [18] and Inoue and Monde [23] are suitable to predict the heat transfer coefficient of the refrigerant mixture R11/R113. However, in case of the non-ideal mixture 1-propanol/water the existing model lead to deviations up to 31 % in comparison to measurement data. In particular, the considered correlations are not able to predict the increase in heat transfer characteristics which is related to the Marangoni effect [28,29]. Therefore, further adaptation and development of the correlations for the heat transfer coefficient for nucleate boiling of mixtures is required in order to improve and

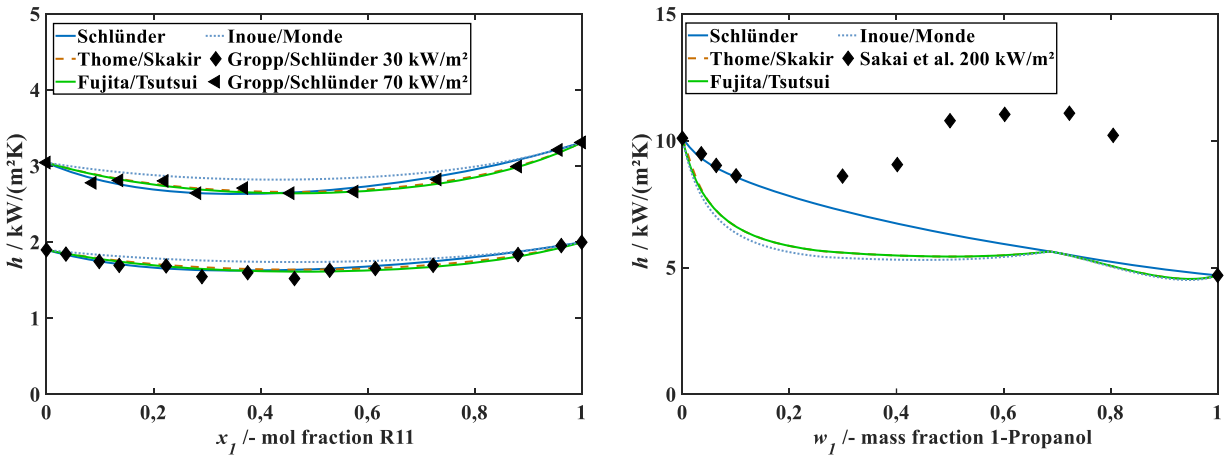

Fig. 3. Experimental nucleate boiling HTC for R11/R113 (left) by Gropp and Schlünder [26] and 1-propanol/water (right) by Sakai et al. [57] mixture at 1 bar in comparison with correlations by Schlünder [21], Thome and Shakir [38], Fujita and Tsutsui [18] and Inoue and Monde [23].

facilitate the prediction. In this work, the implementation of surface tension into an existing correlation approach is focused.

In general, purely empirical fluid-dependent coefficients should be avoided in a correlation to predict the nucleate boiling HTC for mixtures. Furthermore, as few mixture-specific fluid properties as possible are worth striving for as input parameters. The provision and pre-calculation of mixture properties can be a challenging task and lead high uncertainties.

For this purpose, an enhanced correlation (EC) based on the Schlünder [21] and Thome and Shakir [38] correlation is proposed

$$\frac{h_{nb,m}}{h_{id}} = \left[\left(1 + \frac{h_{id}}{\dot{q}}\left[\left(T_{x,i} - T_{S,1}\right) x_1 \sum_{i=1}^{i=n-1} \left(exp(y_i - x_i)\right)^{-1}\right]\right)^{-1}\right]^{m}. \tag{26}$$

The structure is based on Schlünder [21] and Thome and Shakir [38] correlation. However, the consideration of main modifications are:

- Implementing of the local saturation temperature $T_{x,i}$;
- Replacement of the coefficient k_l by the concentration difference $(y_i - x_i)$;
- Consideration of surface tension and density ratio of the pure components by the exponent m

The modifications are explained and justified in detail below.

Regarding the temperature difference in Eq. (26) the local saturation temperature $T_{x,i}$ at the concentration of the volatile component x_1 is set in relation to the saturation temperature of the low boiler $T_{S,1}$ as shown in Fig. 4.

Existing investigations show high uncertainties between measurements and correlations at the AZP. In case of existing models like the ones by Schlünder [21] or Thome and Shakir [38] the applied temperature or concentration differences are zero. This is due to equal compositions and temperatures at the azeotropic point. In the proposed correlation (Eq. (26)), the value of the temperature difference $(T_{x,i} - T_{S,1})$ at the azeotropic point (AZP) is no longer zero. Thus, adjustments can be made in the AZP and the calculated value in the AZP is no longer automatically the averaged mean HTC h_{id}, as it is the case with Schlünder [21] or Thome and Shakir [38], and should thus be adapted to more realistic conditions.

The coefficient k_l in Eq. (17), which is mainly dominated by mixture property data and the mass transfer coefficient β_l, is replaced in the enhanced correlation by the concentration difference $(y_i - x_i)$, which considers the shape of the VLE curve better.

Furthermore, the exponent

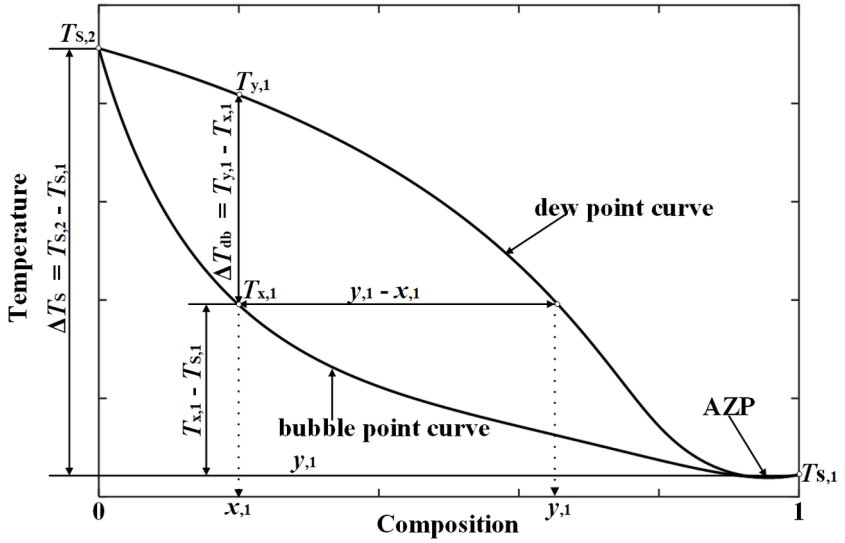

Fig. 4. Vapor-liquid-phase equilibrium of a binary mixture with azeotropic point.

$$m = \frac{\sigma_{2,l}}{\sigma_{1,l}} \frac{\rho_{1,l}}{\rho_{2,l}}. \quad (27)$$

is introduced in Eq. (26). This parameter can be determined by adjusting experimental data, but can also be calculated in advance by applying the surface tensions and densities of the pure fluids at liquid phase. According to Thomson's equation [48], the surface tension has a decisive role for the Marangoni effect [28,29], as well as for the formation of vapor bubbles. Furthermore, Thomson's equation [48] includes a considerable influence on heat transfer characteristics by the liquid density. The densities at gaseous phase were discarded in this approach because previous investigations have indicated that the gas density has a much smaller influence than the liquid density for the calculation of the HTC. Even though Thomson's equation [48] was originally developed for pure fluids, it can be assumed that the dominant variables, such as surface tension or density, also have a significant influence on the boiling process and bubble radius for fluid mixtures. Thus, estimating the exponent m is simple and only requires the fluid properties of the pure fluids. As a result, the Schlünder [21] and Thome and Shakir [38] correlation are significantly simplified because only pure fluid properties and VLE data are taken into account. This eliminates a large source of uncertainty, especially for novel or non-ideal mixtures. Furthermore, possible Marangoni effects can be considered in the calculation by including the surface tensions.

5. Experimental results and discussion

Nucleate boiling heat transfer measurements were carried out for the two mixtures ethanol/water and ethanol/MM. All experimental results were performed at 1 bar and at a heat flux of 40 to 100 kW/m^2.

In order to be able to compare experimental data with correlations, the mean absolute percentage deviation d_{MAP} is calculated according to

$$d_{MAP} = \frac{1}{n} \sum_{1}^{n} \left| \left[\frac{h_{exp} - h_{calc}}{h_{exp}} \right] 100\% \right| \quad (28)$$

for each pure fluid and mixture.

5.1. Pure fluids

To validate the experimental apparatus, measurements were carried out with pure ethanol. The experimental data, which are presented in Fig. 5, are compared with calculated values from the nucleate boiling correlations for pure fluids from Rohsenow [52], Stephan and Abdelsalam [53], and Gorenflo [48,58]. In addition, measurement data from Shen et al. [51] and Fazel et al. [59] for ethanol at 1 bar on a copper surface are included for validation.

Measurements were carried out for Reynolds numbers between 600 and 900 and a heat flux between 40 and 100 kW/m^2. The measurement with a Reynolds number of 900 was started at 100 kW/m^2 and the heat flux density was reduced (q down) to check whether the measurement results were reproducible. The experimental results agree well with the experimental data from Shen et al. [51] and Fazel et al. [59] and show a maximum deviation of 7.8 % for 80 kW/m^2. All other measured results have a mean deviation of less than 5 %. Furthermore, the measurement data can be reproduced very well with the correlations by Rohsenow [52], Stephan and Abdelsalam [53] and Gorenflo [48,58]. Almost all measurement data can be calculated with a deviation of ±10 %. Parameters selected as input for the Rohsenow correlation [52] and related to an ethanol/copper system are $C_{sf} = 0.00079$, $m = 0.33$ and $n = 2.3$ [54].

5.2. Mixtures

In Figs. 6 and 7, the experimental results for the mixtures ethanol/water and ethanol/MM at 1 bar and a heat flux of 40, 80 and 100 kW/m^2 are displayed. In the appendix, the VLE and the calculated $|y_i - x_i|$ and $\Delta T_{db} = T_{y,i} - T_{x,i}$ values are plotted in Figs. 18 and 19. The measurement data are compared with calculated values from the nucleate boiling correlations for mixtures by Schlünder [21], Thome and Shakir [38], Fujita and Tsutsui [18] and Inoue and Monde [23], see Section 3. In order to calculate these mixture correlations, the respective HTC for the pure fluid are required. In this context, the HTC for water was calculated using the Gorenflo correlation in Eq. (11), which showed very good agreement with measurement data for water [48]. For ethanol/MM, the experimental HTCs for the pure fluids were used at $Re = 800$ and are summarized in Table 4 and for validation purposes, experimental data from Fujita and Tsutsui [18], Inoue and Monde [43] and Bonilla and Perry [15] are used for the ethanol/water mixture. For ethanol/MM, no experimental data was found in the literature. Therefore, the HTC for ethanol/MM is only compared to the calculated values.

As it can be seen in Fig. 6, the experimental data for ethanol/water show good agreement with the measurement data from Inoue and Monde [43] and Bonilla and Perry [15] in $a \pm 12$ % range. The measurement data from Fujita and Tsutsui [18] show up to 20 % lower HTCs compared to all other measurement data. This deviation is mainly due to the measurement series at 100 kW/m^2, where a HTC of 6.5 kW/(m^{2}K) for water is measured by Fujita and Tsutsui [11]. The data by Inoue and Monde [43] show a value of 10.2 kW/(m^{2}K) comparable to Bonilla and Perry [15] with 10.4 kW/(m^{2}K) and calculated HTC by the correlation of Gorenflo [48,58] with 10.7 kW/(m^{2}K). For the calculation of the HTC for the investigated mixtures, the HTCs of the pure fluids are

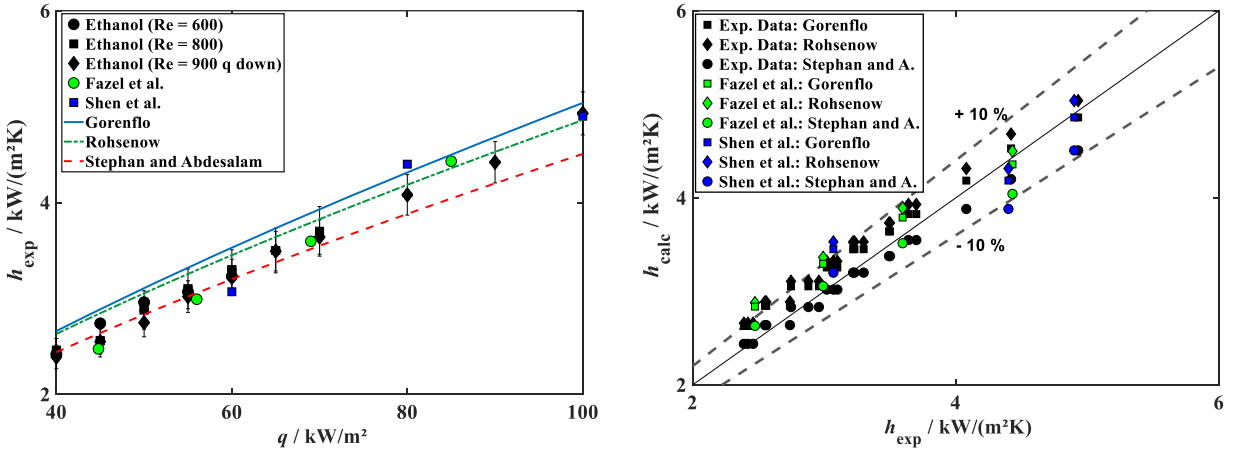

Fig. 5. Experimental nucleate boiling HTC for ethanol with data from Shen et al. [51] and Fazel et al. [59] at 1 bar in comparison of correlations from Rohsenow [52], Stephan and Abdelsalam [53], and Gorenflo [48,58] at a heat flux between 40 and 100 kW/m^2.

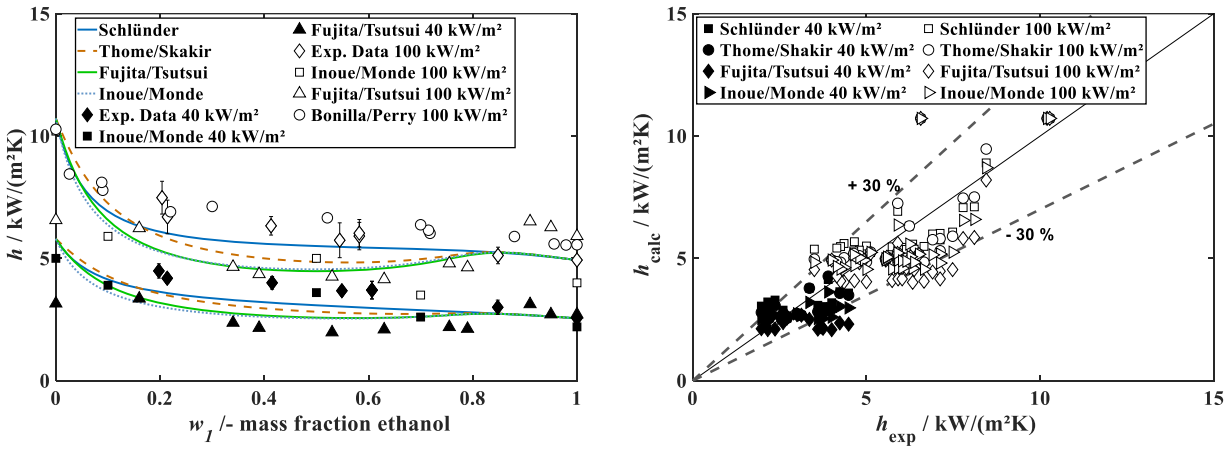

Fig. 6. Experimental nucleate boiling HTC for ethanol/water mixture with data from Fujita and Tsutsui [18], Inoue and Monde [43] and Bonilla and Perry [15] at 1 bar in comparison with correlations from Schlünder [21], Thome and Shakir [38], Fujita and Tsutsui [18] and Inoue and Monde [23] at a heat flux between 40 and 100 kW/m^2.

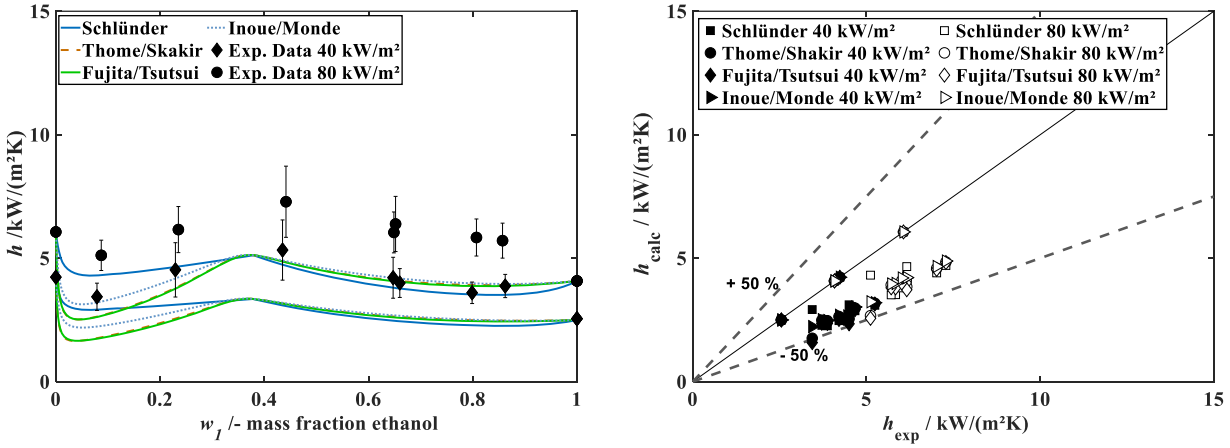

Fig. 7. Experimental nucleate boiling HTC for ethanol/MM mixture at 1 bar in comparison with correlations by Schlünder [21], Thome and Shakir [38], Fujita and Tsutsui [18] and Inoue and Monde [23] at a heat flux between 40 and 80 kW/m^2.

Table 4
HTCs of the pure fluids ethanol, MM and water as a function of heat flux density.

Heat flux kW/m^2	Ethanol W/m^{2}K	MM W/m^{2}K	Water (calculated) W/m^{2}K
40	2552	4230	5800
60	3220	5120	7611
80	4081	6065	9229
100	4933	–	10,720

summarized in Table 4.

The measurement data for water/ethanol can be reproduced qualitatively quite well with the selected correlations. However, the correlations underestimate the measured data. In this context, the Schlünder correlation [21] shows the best agreement with a d_{MAP} of 10.7 %. The largest d_{MAP} is obtained for Fujita and Tsutsui [18] with a mean deviation of 20.6 %.

The experimental HTC for the ethanol/MM mixture in Fig. 7 shows a significantly different course compared to ethanol/water or other mixtures. In particular, a significant increase in the HTC between 0.4 – 1 mass fraction ethanol is observed, compared to the HTC of the pure fluid. Only at a mass fraction lower than 0.4 ethanol (mass fraction), the HTC decreases below the pure fluid of MM. In principle, the effect of increasing HTCs for a mixture was also reported by Sakai et al. [57,60] for their 1-propanol/water mixture. The authors assume that a positive Marangoni effect [28,29] is responsible for this strong increase in the HTC. In their investigations on heat transfer with the Marangoni effect, Straub et al. [61] also demonstrated that the HTC could double due to the Marangoni convection, which shows that the Marangoni effect [28, 29] can have a major influence on the HTC. Overall, it has been shown that the currently existing correlations can reproduce the ethanol/water mixture quite well, but that the deviation also increases with increasing heat flow density. In the case of the ethanol/MM mixture, it can be seen that the correlations do not currently reflect the behavior well.

A detailed discussion taking into account the newly developed correlation is provided in the next chapter.

5.3. Application of the proposed enhanced correlation

In the following, the new proposed enhanced correlation (EC) is compared with the experimental data for ethanol/water and ethanol/MM. Furthermore, the correlation is compared with further measurement data from the literature and the correlations by Schlünder [21], Thome and Shakir [38], Fujita and Tsutsui [18] and Inoue and Monde [23].

5.3.1. Comparison by experimental data ethanol/water and ethanol/MM

Figs. 8 and 9 show the experimental measurement data of ethanol/water and ethanol/MM with the calculated HTCs from the new proposed enhanced correlation at 1 bar and a heat flux of 40 to 100 kW/m^2. As can

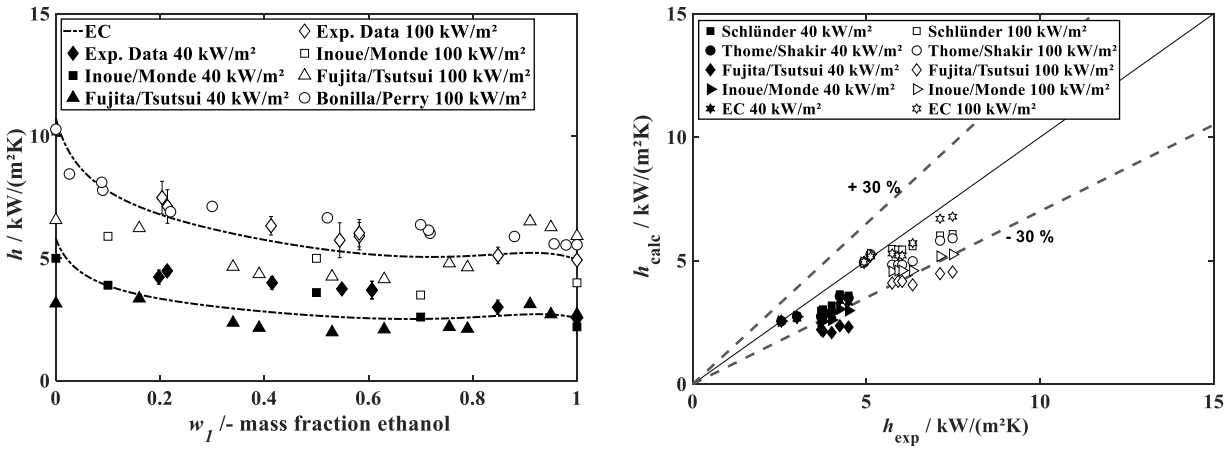

Fig. 8. Experimental nucleate boiling HTC for ethanol/water mixture with data by Fujita and Tsutsui [18], Inoue and Monde [43] and Bonilla and Perry [15] at 1 bar in comparison with the new proposed correlation at heat flux between 40 and 100 kW/m^2.

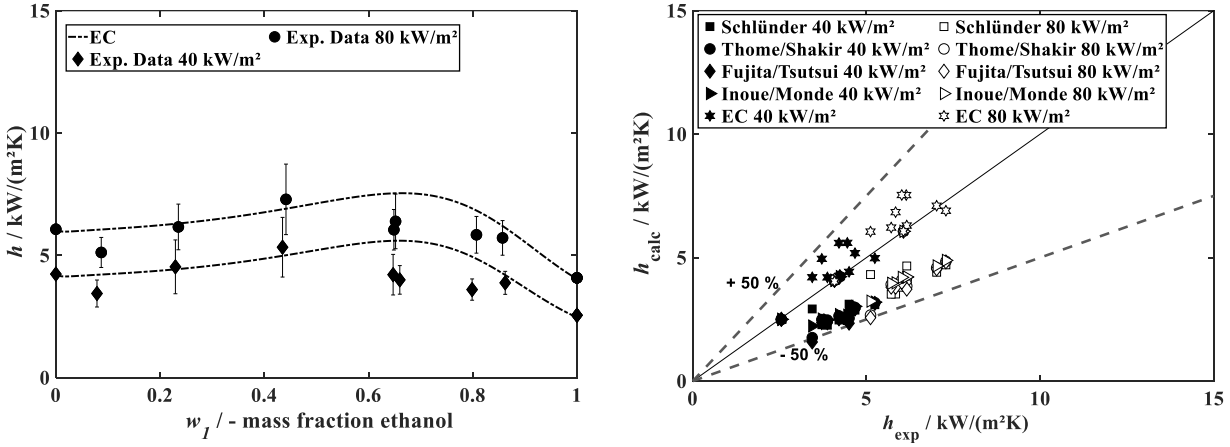

Fig. 9. Experimental nucleate boiling HTC for ethanol/MM mixture at 1 bar in comparison with the new proposed correlation at a heat flux between 40 and 80 kW/m^2.

be clearly seen, the behavior and the course of the measurement data can be reproduced well with the new correlation. In the case of ethanol/MM in particular, the increasing heat transfer coefficient can be reproduced qualitatively very well. Here, possible Marangoni effects [28,29] are represented by considering the surface tension and density ratio.

Only at a mass fraction 0.6 of ethanol in Fig. 9 the correlation overestimates the HTC by 20 %. However, the prediction is significantly improved compared to the alternative correlation as can be seen in Fig. 7. Overall, the mean absolute deviation for the new proposed correlation is 13.3 % for ethanol/water and 11.1 % for ethanol/MM. Evaluating the correlation of Schlünder [21], a mean absolute deviation of 10.7 % for ethanol/water and 34.8 % for ethanol/MM results. The highest deviations are obtained by the correlation of Fujita and Tsutsui [18]. The d_{MAP} is 20.6 % for ethanol/water and 38.8 % for ethanol/MM. In general, a significant improvement by the new developed correlation compared to state-of-art correlations can be determined. A summary of the examined fluids and models and their mean absolute deviations can be found in Table 6.

To conclude this subsection, the well-known mixture of ethanol/water mixture and also ethanol/MM, with a possible positive Marangoni effect [28,29], could be reproduced very well by the new proposed enhanced correlation. The extent to which the developed correlation can also be applied to alternative fluid mixtures is described in the following chapter.

5.3.2. *Comparison with a wide range of various binary mixtures*

In order to justify and prove the relevance of the enhanced correlation, numerous other binary mixtures are applied to the developed approach by literature data. In total, ten binary mixtures were considered with different characteristics, like zeotropic and azeotropic

Table 5
Summary of the considered mixtures including type of mixtures, max. temperature glide ΔT_{db} and the parameter m.

Author	Mixture	Type of mixture	max. ΔT_{db} / K (1 bar)	m
Exp. Data	ethanol/water	azeotropic	11.7	2.71
Exp. Data	ethanol/MM	Azeotropic	19.7	1.69
Sakai et al. [57,60]	1-propanol/water	azeotropic	9.8	2.78
Park et al. [24]	propane/isobutane	zeotropic	8.9	0.84
Gropp and Schlünder [26]	R11/R113	zeotropic	4.8	0.82
Jung et al. [62]	R32/R134a	zeotropic	7.4	0.60
Jung et al. [62]	R125/R134a	zeotropic	5.5	1.24
Stephan and Körner [17]	benzene/toluol	zeotropic	6.7	0.87
Inoue et al. [63,64]	ammonia/water	zeotropic	93.7	1.29
Fujita and Tsutsui [18]	methanol/benzene	zeotropic	15.6	1.06

behavior. As well as mixtures with a small temperature glide ΔT_{db} of 4.8 K for R11/R113 or 93.7 K in case of ammonia/water are included (see Table 5). Furthermore, the listed mixtures and the corresponding HTC measurement data from the various authors are in a pressure range of 1 to 6 bar and a heat flux of 30 to 1000 kW/m^2. VLE data with the calculated $|y_i - x_i|$ and $\Delta T_{db} = T_{y,i} - T_{x,i}$ for all considered mixtures can be seen in the appendix in Figs. 20–27.

As result, Table 6 summarizes the mean absolute deviations d_{MAP} for the HTC for the investigated mixtures compared with the correlations by Schlünder [21], Thome and Shakir [38], Fujita and Tsutsui [18], Inoue and Monde [23] and the proposed EC. In addition, the corresponding measurement data and predicted HTCs are shown in Figs. 10–17 in the appendix for a detailed presentation.

As can be seen in Table 5, the enhanced correlation works very well for a wide range of mixtures, pressure and heat flux densities. In particular, for ethanol/MM and 1-propanol/water mixtures, the HTC is predicted much more precisely compared to the considered existing correlations. The d_{MAP} between the improved correlation and the experimental data is 11.1 % and 5.8 % for these mixtures, and the curve progression of the measurement data for the mixtures could be presented very well. The correlations by Schlünder [21], Thome and Shakir [38], Fujita and Tsutsui [18] and Inoue and Monde [23] show a mean deviation between 21.1 % and 38.8 %.

Very good predictions were obtained for R11/R113, R32/R134a and benzene/toluene with mean absolute deviations below 10 % by the proposed correlation. For R125/R134a, the proposed correlation shows a slightly higher deviation with 13.1 % compared to the established correlations of Inoue and Monde [23], Fujita and Tsutsui [18] and Schlünder [21] show a d_{MAP} between 8.3 % and 11 %. For the high-boiling ammonia/water mixture, all established correlations show a large deviation compared to the measurement data by Inoue et al. [63,64] with 32.6 % for Schlünder [21] to 59.3 % for Inoue and Monde [23]. In contrast, the enhanced correlation leads to the lowest deviation with 23.5 %.

Currently, there is only one mixture type where the HTC is not predicted precisely by the developed correlation. In case of a mixture with a low azeotropic point without a Marangoni effect [28,29], like methanol/benzene. The proposed correlation overestimates compared to the experimental data. In consequence, a mean relative deviation of 31 % results. The state-of-art correlations can reproduce this mixture with deviations between 6.2 % for Schlünder [21] and up to 10.2 % for the Fujita and Tsutsui [18] correlation.

In sum, the new enhanced correlation was tested with ten different binary mixtures in a pressure range of 1 to 6 bar and a heat flux between 30 and 1000 kW/m^2. The overall mean absolute deviation for the binary mixtures $u_{mix,binary}$ for the proposed enhanced correlation is 11.6 %. In contrast, Schlünder [21] shows an overall deviation of 16.1 % while Thome and Shakir [38] have a deviation of 18.6 %. The correlations by Fujita and Tsutsui [18] and Inoue and Monde [23] have mean absolute deviations between 18.5 % and 20.1 %. This proves that the developed enhanced correlation works very well for various mixtures and a wide pressure and heat flow range. Furthermore, in the current form, mixture properties such as density, enthalpy of vaporization, surface tension or mass transfer coefficients can be avoided as input parameters, with the exception of the VLE data, which are essential for all correlations.

Table 6
Comparison of the mean deviation between various mixtures and correlations.

Mixture	S[a]	T/S[b]	F/T[c]	I/M[d]	EC[e]
Ethanol/water	10.7	15.6	20.6	20.5	13.3
Ethanol/MM	34.8	37.4	38.8	34.4	11.1
1-Propanol/water	21.1	30.2	30.2	31.5	5.8
Propane/isobutane	9.5	14.1	13.8	2.9	3.9
R11/R113	1.7	1.7	2.7	4.7	1.8
R32/R134a	30.6	29.4	20.8	18.4	2.6
R125/R134a	8.3	6.2	3.9	11.0	13.1
Benzene/toluol	5.5	6.1	6.6	8.4	4.8
Ammonia/water	32.6	36.8	37.2	59.6	23.5
Methanol/benzene	6.2	8.8	10.2	8.7	31.6
$\overline{u}_{mix,binary}$	**16.1**	**18.6**	**18.5**	**20.1**	**11.6**

[a] S = Schlünder [21]
[b] T/*S* = Thome and Shakir [38]
[c] F/*T* = Fujita and Tsutsui [18].
[d] I/*M* = Inoue and Monde [23].
[e] EC = proposed enhanced correlation.

6. Conclusion

In this study, nucleate boiling heat transfer coefficients were measured on a vertical falling film for ethanol/water and ethanol/MM mixtures at a pressure of 1 bar and for a heat flux between 40 and 100 kW/m^2. The measurement results have been compared with predicted heat transfer coefficients using correlations by Schlünder [21], Thome and Shakir [38], Fujita and Tsutsui[18] and Inoue and Monde [23]. In addition, an enhanced heat transfer correlation has been developed based on the correlations of Schlünder [21] and Thome and Shakir [35] to predict the nucleate boiling heat transfer coefficient of binary mixtures. The proposed correlation provides better prediction accuracy using only VLE data and the density and surface tension of the pure fluids. The HTC measurements for the ethanol/MM mixture show a clearly different curve compared to ethanol/water or other mixtures and a significant increase in the HTC has been observed. The increase in HTC may have been caused by the Marangoni effect [28,29]. None of the correlations by Schlünder [21], Thome and Shakir [38], Fujita and Tsutsui [18] and Inoue and Monde [23] can reproduce the observed shape. The mean absolute deviations range from 34.8 % for the Schlünder correlation [21] up to 38.8 % with the Fujita and Tsutsui[18] correlation. With the developed enhanced heat transfer correlation, both the curve shape and the absolute values of the heat transfer coefficient of ethanol/water and ethanol/MM can be predicted very well. The mean absolute deviation is reduced noticeably to 13.3 % for ethanol/water and 11.1 % for ethanol/MM. For further verification and validation of the enhanced correlation, ten additional binary mixtures are applied in form of literature data. These mixtures include azeotropic as well as zeotropic mixtures and a high variety of temperature glides (4.8 K to 93.7 K). The pressure and heat flux range of the considered data is between 1 and 6 bar and 30 to 1000 kW/m^2. Overall, a mean absolute deviation of 11.6 % for the proposed enhanced correlation is obtained, which is considerably lower than the existing correlations by which lead to deviations between 16.1 % and 20.1 %.

Future work should focus on mixtures with an azeotropic point, which appears under the volatile component, without the Marangoni effect [28,29]. Since the applicability of the new developed correlation is limited for these mixtures adjustments may be needed. Furthermore, reliable VLE data are one of the most important factors to determine HTCs for mixtures. In order to further improve the developed correlation or to predict multi-component mixtures, additional VLE data will be required.

CRediT authorship contribution statement

Zlatan Arnautovic: Writing – original draft, Visualization, Resources, Methodology, Investigation, Formal analysis, Data curation, Conceptualization. **Matthias Welzl:** Writing – review & editing, Investigation, Formal analysis, Data curation. **Florian Heberle:** Writing – review & editing, Formal analysis. **Dieter Brüggemann:** Writing – review & editing, Supervision.

Declaration of competing interest

The authors declare that they have no known competing financial interests or personal relationships that could have appeared to influence the work reported in this paper. The authors confirm that this

manuscript has not been published elsewhere and is not under consideration by another journal. This work was supported by the Deutsche Forschungsgemeinschaft (DFG, German Research

Data availability

Data will be made available on request.

Funding

The authors of this work gratefully acknowledge the financial support provided by the Deutsche Forschungsgemeinschaft (DFG, German Research Foundation – Project number: 401366378).

Appendix A: Uncertainties

Table 7
Uncertainty contributions for the heat transfer coefficient.

Input variables $x(i)$		$u(i)$	Source	Value
Geometric variables				
Inner diameter	D_{in}	$u(D_{in})$	caliper gauge	0.029 mm
Outer diameter	$D_{w,a}$	$u(D_{w,a})$	caliper gauge	0.029 mm
Diameter with solder	$D_{w,in}$	$u(D_{w,in})$	caliper gauge	0.029 mm
Position sensor	D_m	$u(D_m)$	assumption	0.2 mm
Tolerance heating cartridge	L	$u(L)$	manufacturer	4.2 mm
Measurement instrument				
Heat flux	$\dot{Q}$	$u(\dot{Q})$	calculated	$f(P_{el})$
Temperature sensor Pt-100	$T_{in,j}$	$u(T_{in,j},1)$	LC—Cal-LRT	0.01 K
Temperature sensor Pt-100	$T_{in,j}$	$u(T_{in,j},2)$	measuring module	0.029 K
Pressure sensor	p	$u_1(p)$	manufacturer	11 mbar
Pressure sensor	p	$u_2(p)$	measuring module	0.76 mbar
Thermophysical properties				
Thermal conductivity solder	k_{sol}	$u(k_{sol})$	literature	1.3 W/(mK)
Thermal conductivity copper	k_c	$u(k_{in,a})$	calculated	±4.5 % MW
Saturation temperature (concentration deviation)	T_s	$u_1(T_s)$	NRTL	$f(x_1)$
Saturation temperature (VLE)	T_s	$u_2(T_s)$	NRTL	0.07 – 0.96 K
Saturation temperature (p)	T_s	$u_3(T_s)$	NRTL	$f(p)$

Appendix B: Heat transfer coefficient data

Measurement Data compared with calculated HTC from Schlünder, Thome and Shakir, Fujita and Tsutsui and the new developed enhanced correlation

1-propanol/water

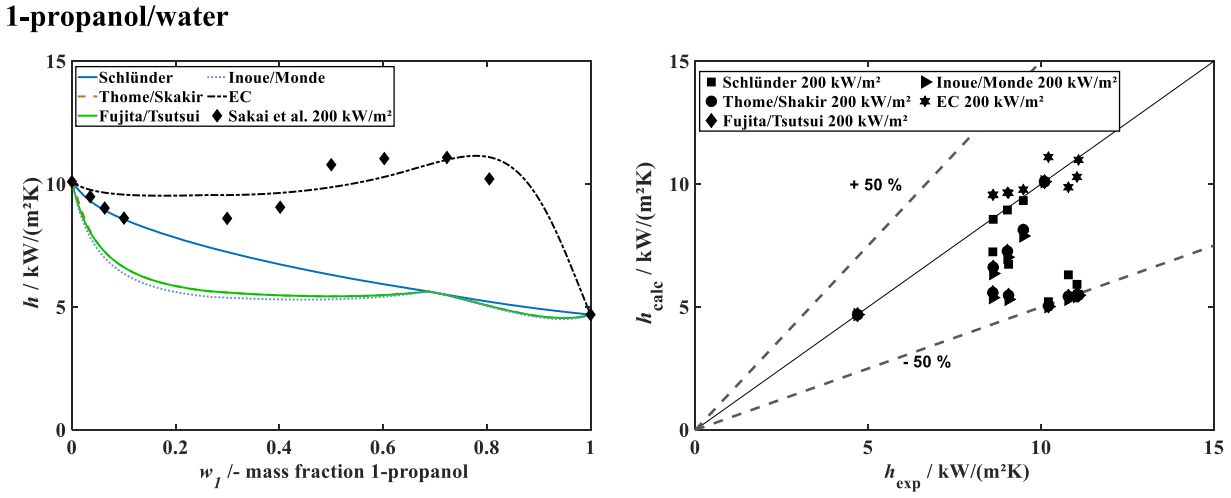

Fig. 10. Experimental nucleate boiling HTC for 1-propanol/water mixture with data by Sakai et al. [57,60] at 1 bar in comparison of correlations from Schlünder [21], Thome and Shakir [38], Fujita and Tsutsui [18] and Inoue and Monde [23] and the enhanced correlation with a heat flux of 200 kW/m^2.

Propane/isobutane

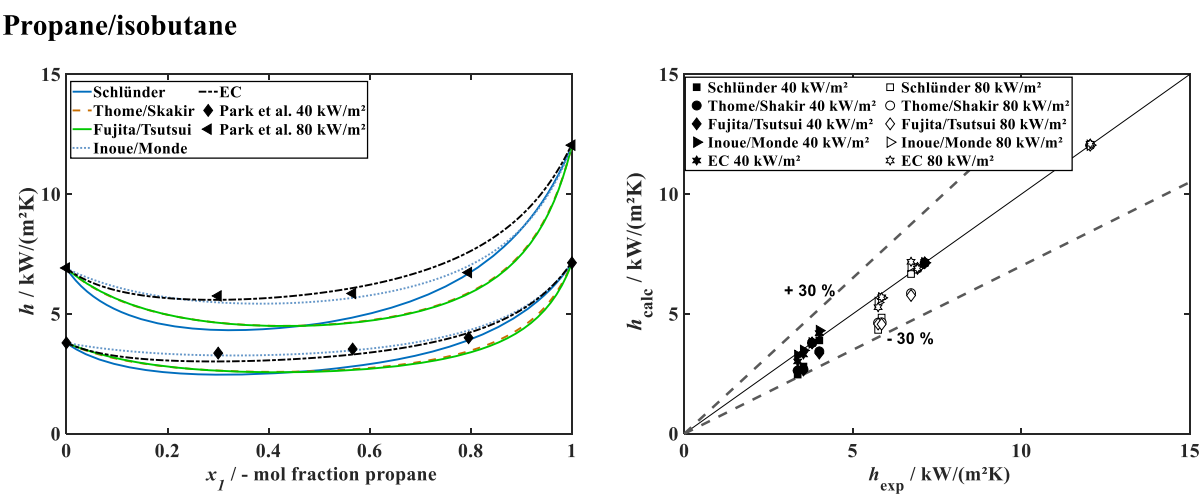

Fig. 11. Experimental nucleate boiling HTC for propane/isobutane mixture with data by Park et al. [24] at 1 bar in comparison of correlations from Schlünder [21], Thome and Shakir [38], Fujita and Tsutsui [18] and Inoue and Monde [23] and the enhanced correlation with a heat flux between 40 and 80 kW/m^2.

R11/R113

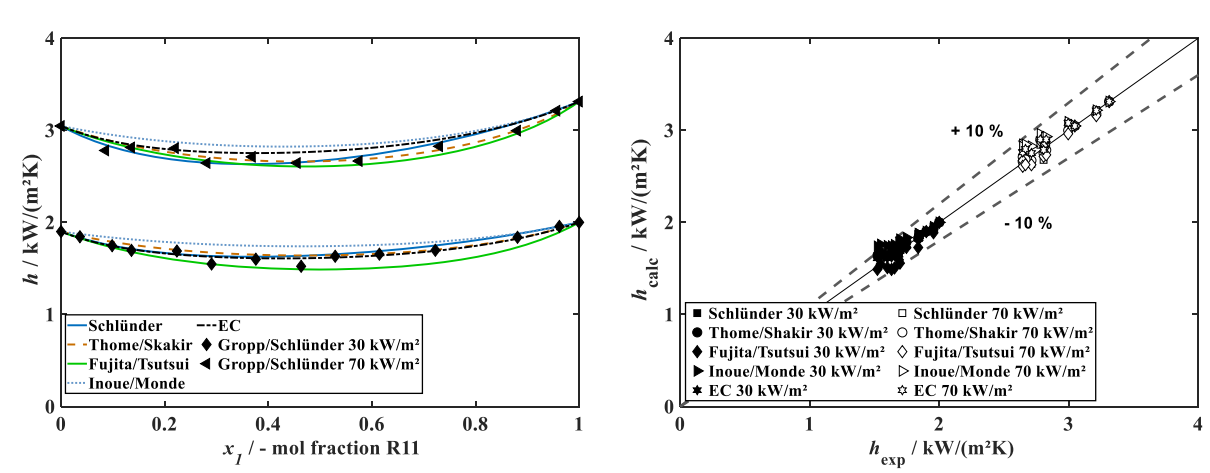

Fig. 12. Experimental nucleate boiling HTC R11/R113 mixture with data by Gropp and Schlünder [26] at 1 bar in comparison of correlations by Schlünder [21], Thome and Shakir [38], Fujita and Tsutsui [18] and Inoue and Monde [23] and the enhanced correlation with a heat flux between 30 and 70 kW/m^2.

R32/R134a

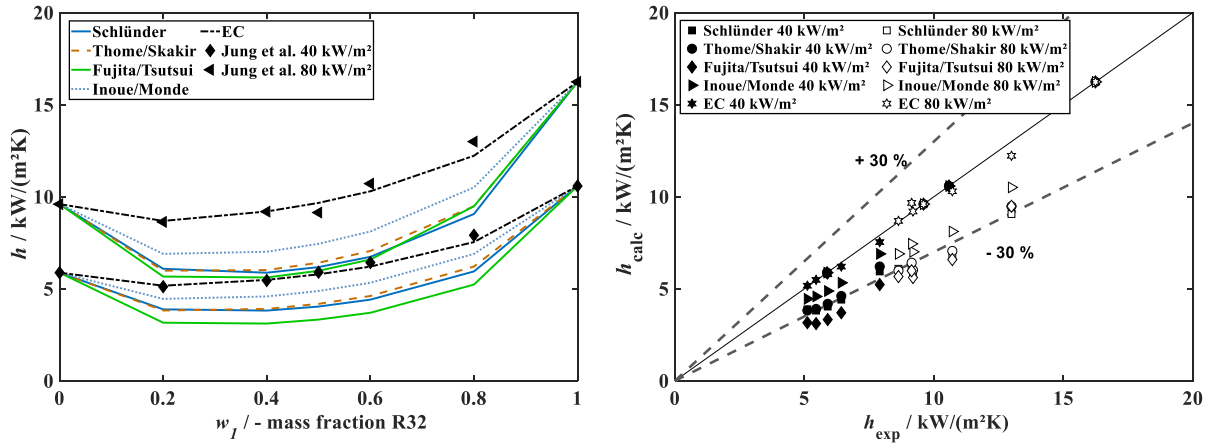

Fig. 13. Experimental nucleate boiling HTC R32/R134a mixture with data by Jung et al. [62] between 5.8 to 9.4 bar in comparison of correlations by Schlünder [21], Thome and Shakir [38], Fujita and Tsutsui [18] and Inoue and Monde [23] and the enhanced correlation with a heat flux between 40 and 80 kW/m^2.

R125/R134a

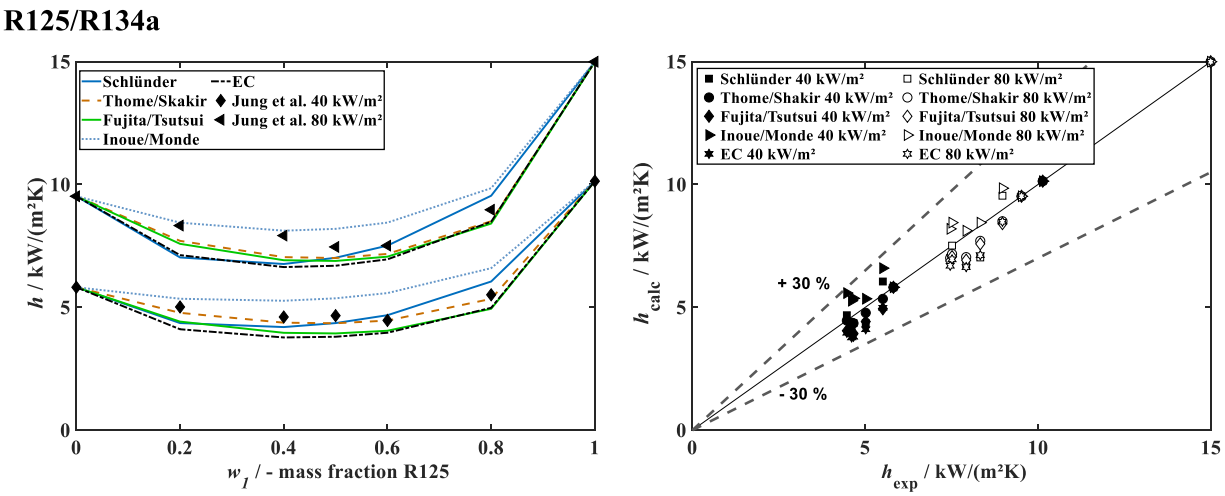

Fig. 14. Experimental nucleate boiling HTC R125/R134a mixture with data by Jung et al. [62] between 4.6 to 7.3 bar in comparison of correlations by Schlünder [21], Thome and Shakir [38], Fujita and Tsutsui [18] and Inoue and Monde [23] and the enhanced correlation with a heat flux between 40 and 80 kW/m^2.

Benzene/toluol

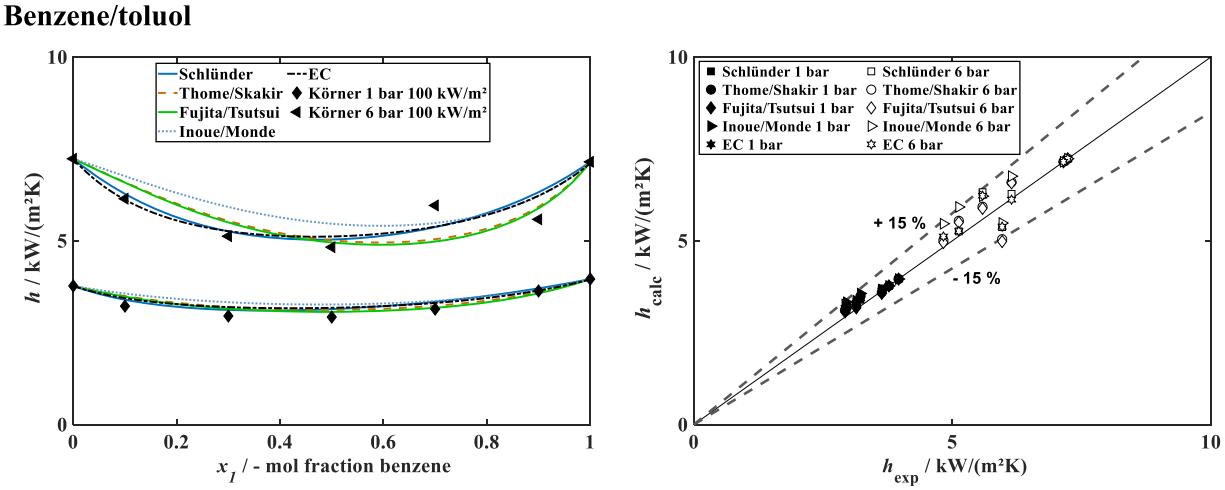

Fig. 15. Experimental nucleate boiling benzene/toluol mixture with data by Stephan and Körner [17] between 1 and 6 bar in comparison of correlations by Schlünder [21], Thome and Shakir [38], Fujita and Tsutsui [18] and Inoue and Monde [23] and the enhanced correlation with a heat flux of 100 kW/m^2.

Ammonia/water

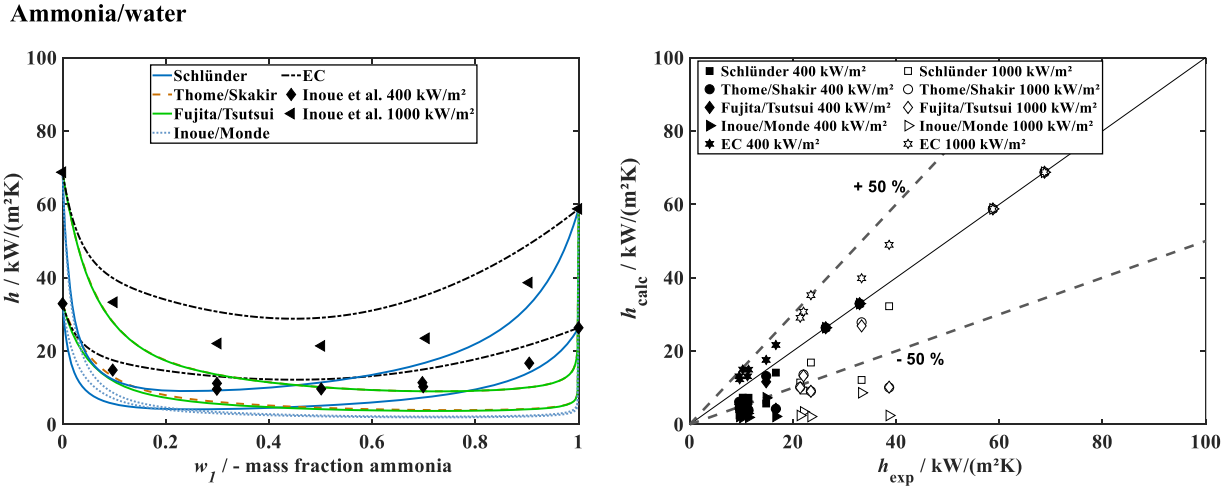

Fig. 16. Experimental nucleate boiling ammonia/water mixture with data by Inoue et al. [63,64] at 4 bar in comparison of correlations by Schlünder [21], Thome and Shakir [38], Fujita and Tsutsui [18] and Inoue and Monde [23] and the enhanced correlation with a heat flux between 400 and 1000 kW/m^2.

Methanol/benzene

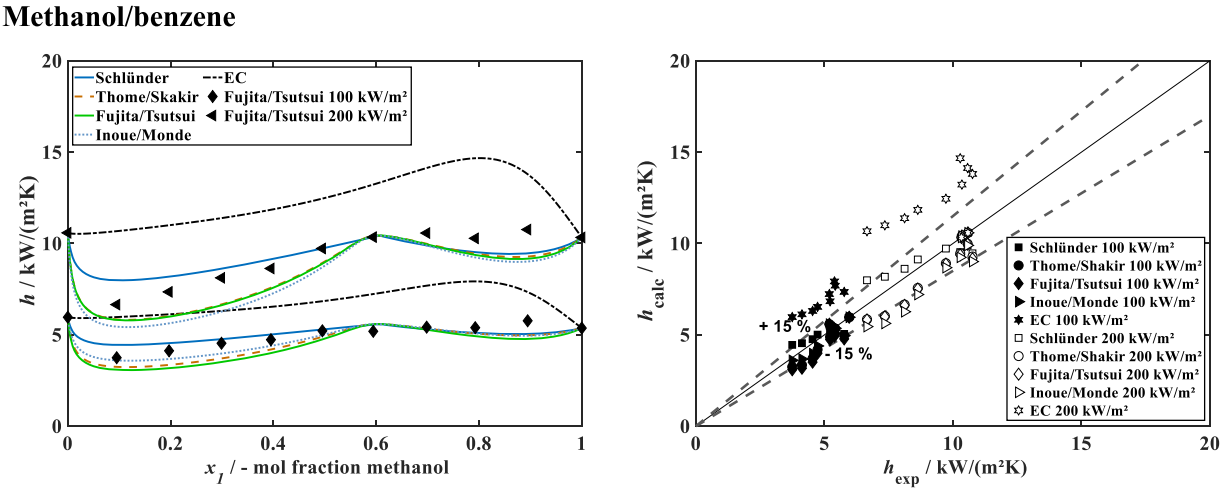

Fig. 17. Experimental nucleate boiling methanol/benzene mixture with data by Fujita and Tsutsui [18] at 1 bar in comparison of correlations by Schlünder [21], Thome and Shakir [38], Fujita and Tsutsui [18] and Inoue and Monde [23] and the enhanced correlation with a heat flux between 100 and 200 kW/m^2.

Appendix C: Vapor-Liquid-Equilibria data

VLE data were calculated using the g^E – model NRTL.

ethanol/water

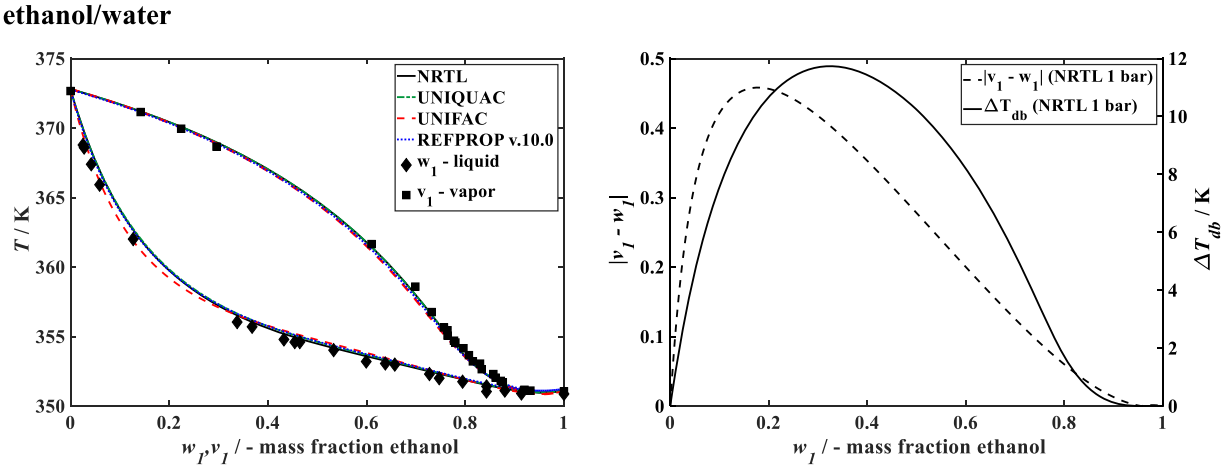

Fig. 18. VLE of ethanol/water with $|\boldsymbol{v}_1 - \boldsymbol{w}_1|$ and $\boldsymbol{\Delta T_{db}}$ at 1 bar.

ethanol/MM

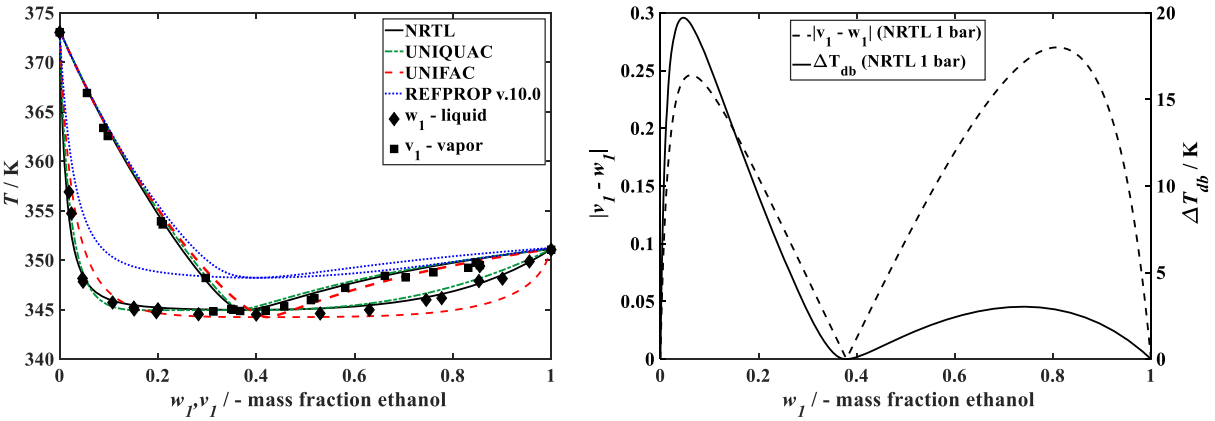

Fig. 19. VLE of ethanol/MM with $|\boldsymbol{v}_1 - \boldsymbol{w}_1|$ and $\boldsymbol{\Delta T_{db}}$ at 1 bar.

1-propanol/water

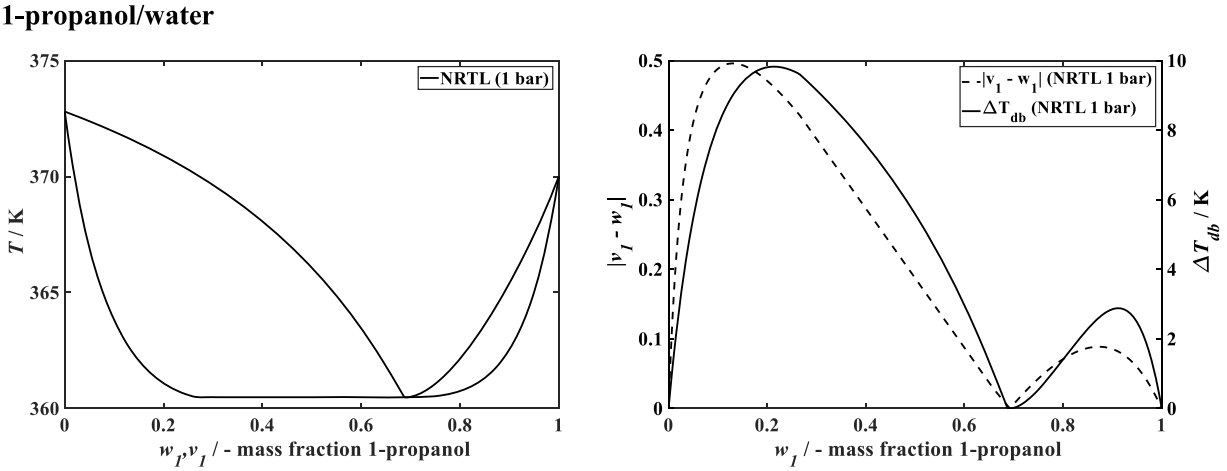

Fig. 20. VLE of 1-propanol/water with $|\boldsymbol{v}_1 - \boldsymbol{w}_1|$ and $\boldsymbol{\Delta T_{db}}$ at 1 bar.

propane/isobutane

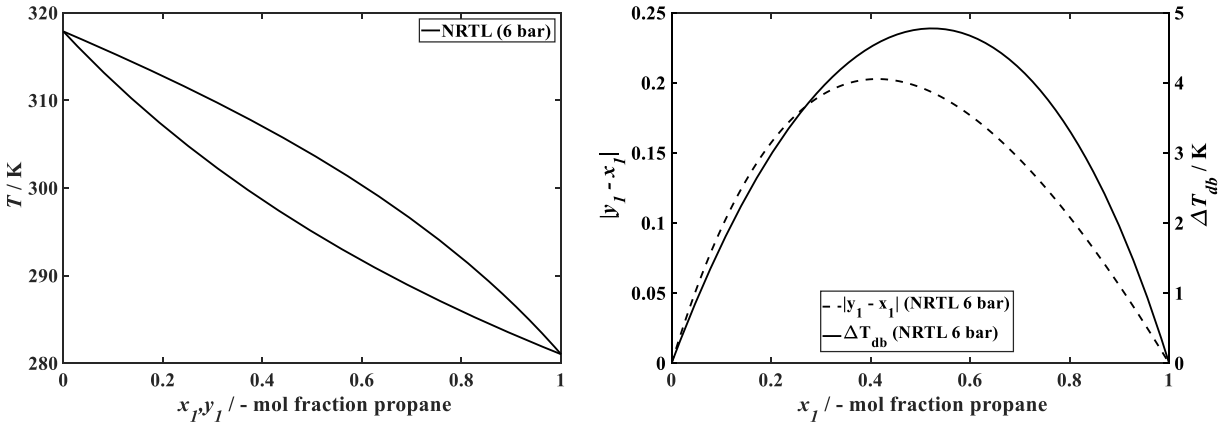

Fig. 21. VLE of propane/isobutane with $|\boldsymbol{y}_1 - \boldsymbol{x}_1|$ and $\boldsymbol{\Delta T_{db}}$ at 6 bar.

R11/R113

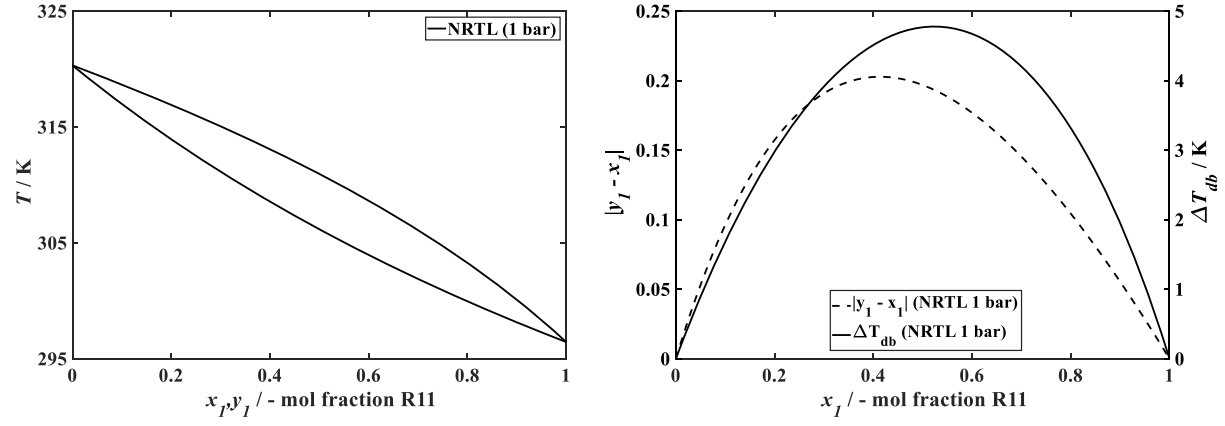

Fig. 22. VLE of R11/R113 with $|\boldsymbol{y}_1 - \boldsymbol{x}_1|$ and $\boldsymbol{\Delta T_{db}}$ at 1 bar.

R32/R134a

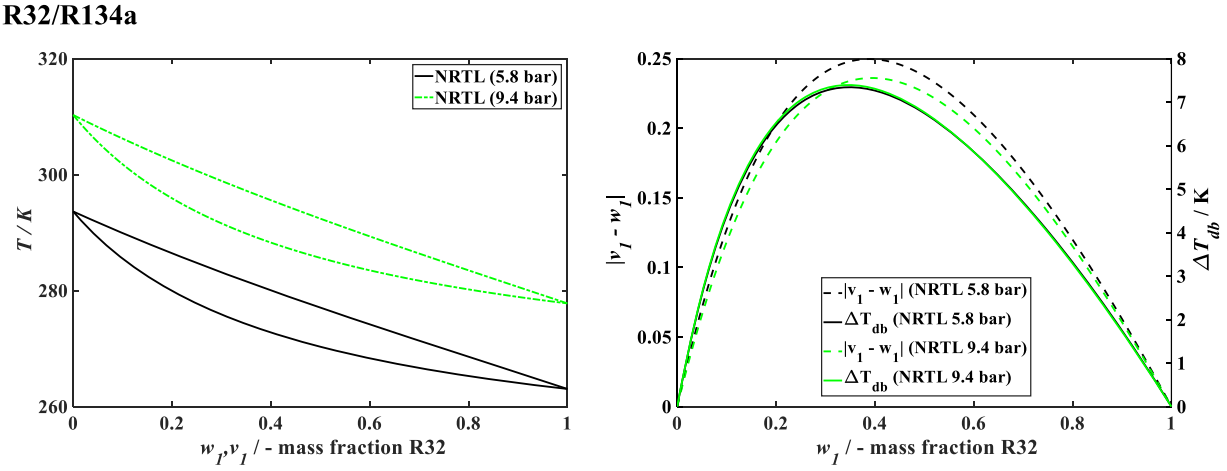

Fig. 23. VLE of R32/R134a with $|\boldsymbol{v}_1 - \boldsymbol{w}_1|$ and $\boldsymbol{\Delta T_{db}}$ at 5.8 and 9.4 bar.

R125/R134a

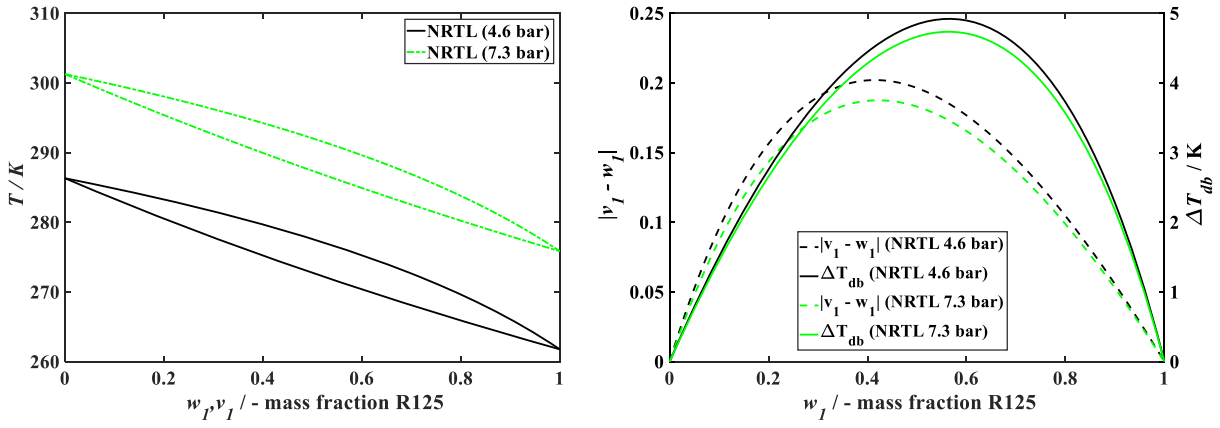

Fig. 24. VLE of R125/R134a with $|\boldsymbol{v}_1 - \boldsymbol{w}_1|$ and $\boldsymbol{\Delta T_{db}}$ at 4.6 and 7.3 bar.

benzene/toluol

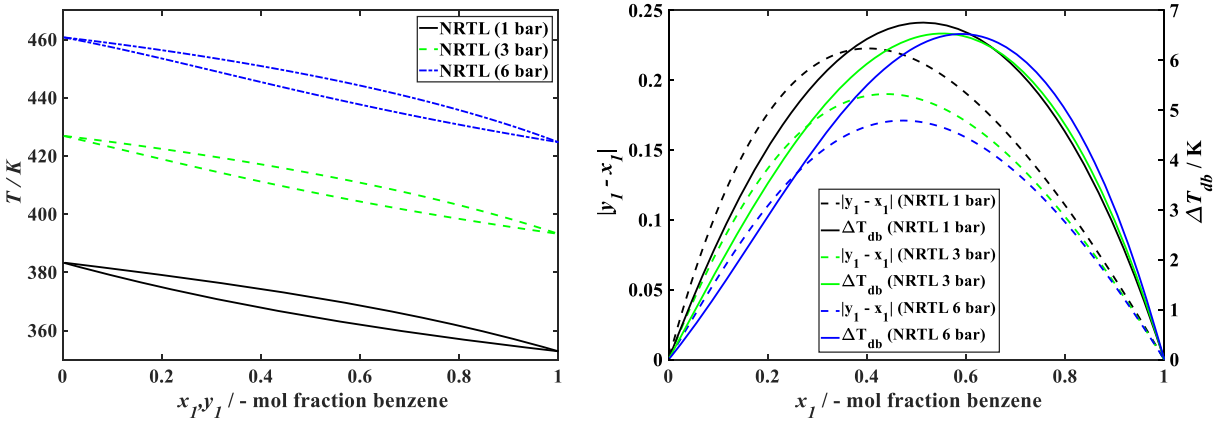

Fig. 25. VLE of benzol/toluol with $|\boldsymbol{y}_1 - \boldsymbol{x}_1|$ and $\boldsymbol{\Delta T_{db}}$ at 1,3,6 bar.

ammonia/water

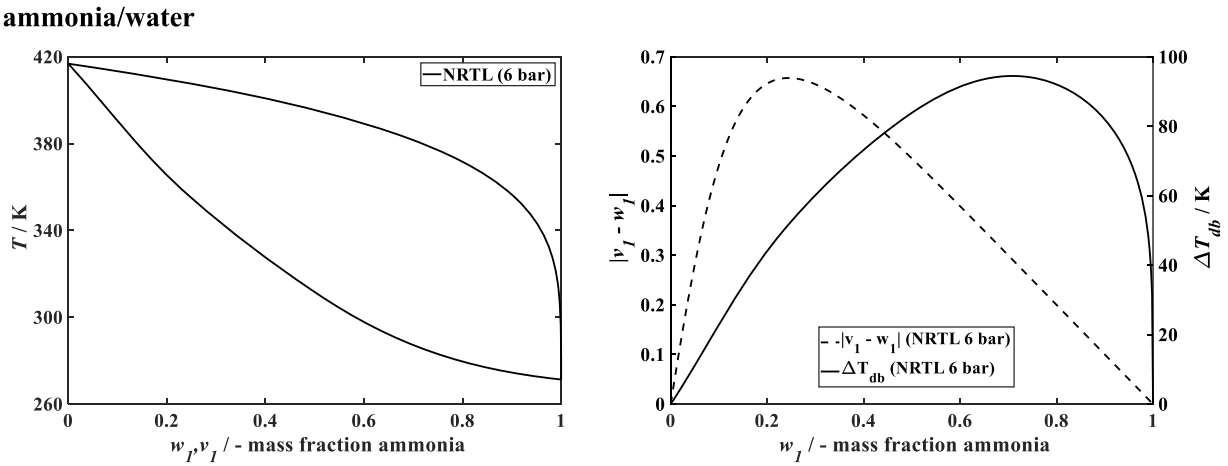

Fig. 26. VLE of ammonia/water with $|\boldsymbol{v}_1 - \boldsymbol{w}_1|$ and $\boldsymbol{\Delta T_{db}}$ at 6 bar.

methanol/benzene

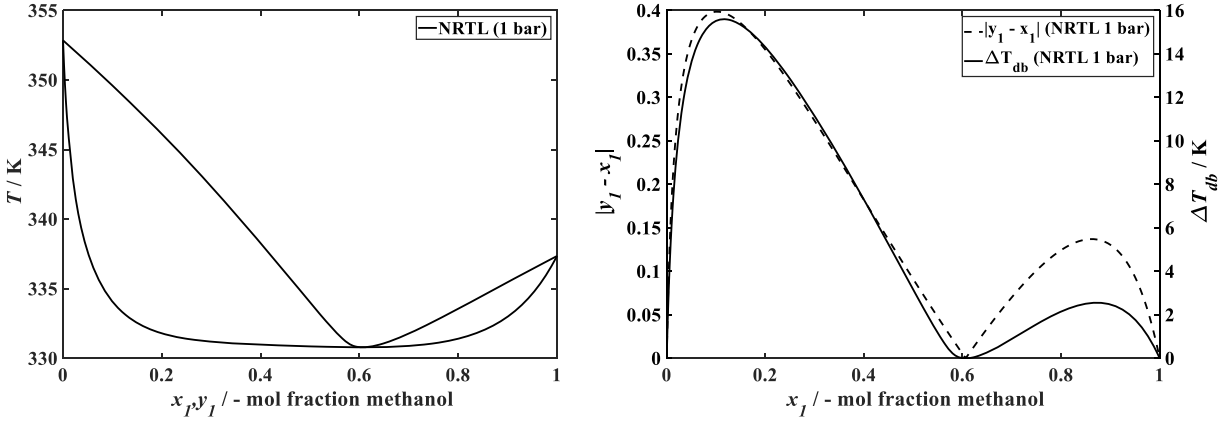

Fig. 27. VLE of methanol/benzene with $|\boldsymbol{y}_1 - \boldsymbol{x}_1|$ and $\boldsymbol{\Delta T_{db}}$ at 1 bar.

References

[1] L. Ji, S.K. Shukla, Z. Zuo, X. Lu, X. Ji, C. Wang, An overview of the progress of new working pairs in absorption heat pumps, Energy Rep. 9 (2023) 703–729, https://doi.org/10.1016/j.egyr.2022.11.143.

[2] R. Radermacher, Y. Hwang, Vapor Compression Heat Pumps with Refrigerant Mixtures, CRC Press, 2005.

[3] S.Newaz Kazi (Ed.), Low-Temperature Technologies and Applications, IntechOpen, 2022.

[4] S. Pandian Ebenezer, Refrigerant mixtures, in: S.Newaz Kazi (Ed.), Low-Temperature Technologies and Applications, IntechOpen, 2022.

[5] M. Schulz, D. Kourkoulas, Regulation (EU) No 517/2014 of the European parliament and of the council of 16 April 2014 on fluorinated greenhouse gases and Regulation (EC) No 842/2006, Off. J. Eur. Union 2014 (2014) 517.

[6] M. Chys, M. van den Broek, B. Vanslambrouck, M. de Paepe, Potential of zeotropic mixtures as working fluids in organic rankine cycles, Energy 44 (2012) 623–632, https://doi.org/10.1016/j.energy.2012.05.030.

[7] M. Bai, L. Zhao, R. Zhao, Review on applications of zeotropic mixtures, J. Therm. Sci. 31 (2022) 285–307, https://doi.org/10.1007/s11630-022-1569-x.

[8] A. Modi, F. Haglind, A review of recent research on the use of zeotropic mixtures in power generation systems, Energy Convers. Manage. 138 (2017) 603–626, https://doi.org/10.1016/j.enconman.2017.02.032.

[9] Y. Heredia-Aricapa, J.M. Belman-Flores, A. Mota-Babiloni, J. Serrano-Arellano, J. J. García-Pabón, Overview of low GWP mixtures for the replacement of HFC refrigerants: r134a, R404A and R410A, Int. J. Refriger. 111 (2020) 113–123, https://doi.org/10.1016/j.ijrefrig.2019.11.012.

[10] W. Wang, L. Tian, L. Shi, X. Dai, Experimental and simulation analysis of siloxane mixtures used in organic rankine cycle with thermal stability limits, Processes 11 (2023) 2108, https://doi.org/10.3390/pr11072108.

[11] T. Weith, F. Heberle, M. Preißinger, D. Brüggemann, Performance of siloxane mixtures in a high-temperature organic rankine cycle considering the heat transfer characteristics during evaporation, Energies. (Basel) 7 (2014) 5548–5565, https://doi.org/10.3390/en7095548.

[12] F. Heberle, M. Preißinger, D. Brüggemann, Zeotropic mixtures as working fluids in organic rankine cycles for low-enthalpy geothermal resources, Renew. Energy 37 (2012) 364–370, https://doi.org/10.1016/j.renene.2011.06.044.

[13] J.G. Andreasen, E. Baldasso, M.R. Kærn, T. Weith, F. Heberle, D. Brüggemann, F. Haglind, Techno-economic feasibility analysis of zeotropic mixtures and pure fluids for organic rankine cycle systems, Appl. Therm. Eng. 192 (2021) 116791, https://doi.org/10.1016/j.applthermaleng.2021.116791.

[14] J.G. Andreasen, U. Larsen, T. Knudsen, F. Haglind, Design and optimization of a novel organic rankine cycle with improved boiling process, Energy 91 (2015) 48–59, https://doi.org/10.1016/j.energy.2015.06.122.

[15] C.F. Bonilla, C.W. Perry, Heat transmission to boiling mixtures, Am. Inst. Chem. Eng. J. (1941) 685–705.

[16] W.F. Calus, D.J. Leonidopoulos, Pool boiling—Binary liquid mixtures, Int. J. Heat. Mass Transf. 17 (1974) 249–256, https://doi.org/10.1016/0017-9310(74)90086-6.

[17] K. Stephan, M. Körner, Berechnung des wärmeübergangs verdampfender binärer flüssigkeitsgemische, Chem. Ing. Tech. 41 (1969) 409–417, https://doi.org/10.1002/cite.330410702.

[18] Y. Fujita, M. Tsutsui, Heat transfer in nucleate pool boiling of binary mixtures, Int. J. Heat. Mass Transf. 37 (1994) 291–302, https://doi.org/10.1016/0017-9310(94)90030-2.
[19] J.R. Thome, Prediction of binary mixture boiling heat transfer coefficients using only phase equilibrium data, Int. J. Heat. Mass Transf. 26 (1983) 965–974, https://doi.org/10.1016/S0017-9310(83)80121-5.
[20] H.C. Ünal, Prediction of nucleate pool boiling heat transfer coefficients for binary mixtures, Int. J. Heat. Mass Transf. 29 (1986) 637–640, https://doi.org/10.1016/0017-9310(86)90096-7.
[21] E.U. Schlunder, Heat transfer in nucleate boiling of mixtures, in: Proceeding of International Heat Transfer Conference 8, Connecticut, Begellhouse, Connecticut, 1986.
[22] Peter Preußer, Wärmeübergang beim verdampfen binärer und ternärer Flüssigkeitsgemische. Dissertation, 1978.
[23] T. Inoue, M. Monde, Nucleate pool boiling heat transfer in binary mixtures, Wärme- Stoffübertr. 29 (1994) 171–180, https://doi.org/10.1007/BF01548601.
[24] K.-J. Park, D. Jung, Nucleate boiling heat transfer coefficients of mixtures containing propane, isobutane and HFC134a, J. Mech. Sci. Technol. 20 (2006) 399–408, https://doi.org/10.1007/BF02917523.
[25] J. Li, L. Lin, S. Li, Z. Yang, Y. Duan, Experimental study on nucleate pool boiling heat transfer characteristics of R32 + R1234yf binary mixtures, Appl. Therm. Eng. 205 (2022) 118047, https://doi.org/10.1016/j.applthermaleng.2022.118047.
[26] U. Gropp, E.U. Schlünder, The influence of liquid-side mass transfer on heat transfer and selectivity during surface and nucleate boiling of liquid mixtures in a falling film, Chem. Eng. Process.: Process Intensif. 20 (1986) 103–114, https://doi.org/10.1016/0255-2701(86)85014-0.
[27] J. Xu, Y. Wang, R. Yang, W. Liu, H. Wu, Y. Ding, Y. Li, A review of boiling heat transfer characteristics in binary mixtures, Int. J. Heat. Mass Transf. 164 (2021) 120570, https://doi.org/10.1016/j.ijheatmasstransfer.2020.120570.
[28] C.G.M. Marangoni, Sull'espansione Delle Goccie D'un Liquido Galleggianti Sulla Superfice Di Altro Liquido, Fratelli Fusi, 1865.
[29] A.V. Getling, A.V. Getling, Rayleigh-Bénard convection: Structures and Dynamics, World Scientific, Singapore, 1998.
[30] T. Fujita, T. Ueda, Heat transfer to falling liquid films and film breakdown—I, Int. J. Heat. Mass Transf. 21 (1978) 97–108, https://doi.org/10.1016/0017-9310(78)90212-0.
[31] F. Toshihiko, U. Tatsuhiro, Heat transfer to falling liquid films and film breakdown—II, Int. J. Heat. Mass Transf. 21 (1978) 109–118, https://doi.org/10.1016/0017-9310(78)90213-2.
[32] F. Weise, S. Scholl, Fluiddynamik und Wärmeübergang bei der fallfilmverdampfung von reinstoffen mit hohen Prandtl-Zahlen, Chem. Ing. Tech. 79 (2007) 1145–1153, https://doi.org/10.1002/cite.200700028.
[33] J. Fernández-Seara, Á.Á. Pardiñas, Refrigerant falling film evaporation review: description, fluid dynamics and heat transfer, Appl. Therm. Eng. 64 (2014) 155–171, https://doi.org/10.1016/j.applthermaleng.2013.11.023.
[34] Y. Fujita, M. Tsutsui, Experimental investigation of falling film evaporation on horizontal tubes, Heat Trans. Jpn. Res. 27 (1998) 609–618, https://doi.org/10.1002/(SICI)1520-6556(1998)27:8<609:AID-HTJ5 3.0.CO;2-N.
[35] A.A. Alhusseini, K. Tuzla, J.C. Chen, Falling film evaporation of single component liquids, Int. J. Heat. Mass Transf. 41 (1998) 1623–1632, https://doi.org/10.1016/S0017-9310(97)00308-6.
[36] Y. Hu, S. Chen, J. Huang, M. Song, Marangoni effect on pool boiling heat transfer enhancement of self-rewetting fluid, Int. J. Heat. Mass Transf. 127 (2018) 1263–1270, https://doi.org/10.1016/j.ijheatmasstransfer.2018.08.003.
[37] K. Namura, K. Nakajima, M. Suzuki, Investigation of transition from thermal- to solutal-Marangoni flow in dilute alcohol/water mixtures using nano-plasmonic heaters, Nanotechnology 29 (2018) 65201, https://doi.org/10.1088/1361-6528/aaa260.
[38] J.R. Thome, S. Shakir, A new correlation for nucleate pool boiling of aqueous mixtures. Heat Transfer, Pittsburgh, 1987, p. 1987.
[39] Z. Arnautovic, T. Weith, F. Heberle, D. Brüggemann, Isobaric vapor-liquid equilibrium for ethanol/water and binary linear siloxane mixtures at 100 kPa, Fluid. Phase Equilib. 556 (2022) 113371, https://doi.org/10.1016/j.fluid.2021.113371.
[40] Z. Arnautovic, S. Kutzner, T. Weith, F. Heberle, D. Brüggemann, Density and viscosity of linear siloxanes and their mixtures, J. Chem. Eng. Data 68 (2023) 314–329, https://doi.org/10.1021/acs.jced.2c00590.
[41] G. ANGELINO, P. COLONNADIPALIANO, Multicomponent working fluids for organic rankine cycles (ORCs), Energy 23 (1998) 449–463, https://doi.org/10.1016/S0360-5442(98)00009-7.
[42] W.K.A. Abbas, E. Baumhögger, J. Vrabec, Experimental investigation of organic Rankine cycle performance using alkanes or hexamethyldisiloxane as a working fluid, Energy Convers. Manage.: X 15 (2022) 100244, https://doi.org/10.1016/j.ecmx.2022.100244.
[43] T. Inoue, Y. Teruya, M. Ishii, M. Monde, Enhancement of pool boiling heat transfer in water and ethanol/water mixtures (effect of surface-active agent), Heat Trans. Asian Res. 33 (2004) 229–244, https://doi.org/10.1002/htj.20010.
[44] Experimental study of nucleate pool boiling heat transfer on a copper tube for low gwp refrigerants, in: M. Welzl, T. Weith, F. Heberle, D. Brüggemann (Eds.), The Second Pacific Rim Thermal Engineering Conference (PRTEC2019), 2019.
[45] M. Welzl, Untersuchung Des Wärmeübergangs und Der Leistungsabgabe bei Einsatz von Arbeitsmedien mit Geringem Treibhauspotenzial im Organic Rankine Cycle, Dissertation, Universität Bayreuth, Berlin, 2023.
[46] Bruker, FT-IR Spectrometers INVENIO, 2023. https://www.bruker.com/en/products-and-solutions/infrared-and-raman/ft-ir-research-spectrometers/invenio-ft-ir-spectrometer.html.
[47] ISO/IEC GUIDE 98-3:2008, uncertainty of measurement — Part 3: guide to the expression of uncertainty in measurement, 2008.
[48] P. Stephan, S. Kabelac, M. Kind, D. Mewes, K. Schaber, T. Wetzel, VDI-Wärmeatlas, Springer Berlin Heidelberg, Berlin, Heidelberg, 2019.
[49] N. Nishikawa, Heat transfer in nucleate boiling, Trans. Japan. Soe. Mech. Engrs. (1956) 557–561.
[50] A. Vieira da Silva Oliveira, R. Gonçalves dos Santos, G. Alegre, Accuracy of boiling correlations on nucleate boiling with ethanol using a thin platinum wire at different pressures, in: Procceedings of the 16th Brazilian Congress of Thermal Sciences and Engineering, ABCM, 2016, 11/07/.
[51] B. Shen, T. Hamazaki, W. Ma, N. Iwata, S. Hidaka, A. Takahara, K. Takahashi, Y. Takata, Enhanced pool boiling of ethanol on wettability-patterned surfaces, Appl. Therm. Eng. 149 (2019) 325–331, https://doi.org/10.1016/j.applthermaleng.2018.12.049.
[52] W.M. Rohsenow, Boiling, Annu. Rev. Fluid Mech. 3 (1971) 211–236, https://doi.org/10.1146/annurev.fl.03.010171.001235.
[53] K. Stephan, M. Abdelsalam, Heat-transfer correlations for natural convection boiling, Int. J. Heat. Mass Transf. 23 (1980) 73–87, https://doi.org/10.1016/0017-9310(80)90140-4.
[54] I.l. Pioro, Experimental evaluation of constants for the Rohsenow pool boiling correlation, Int. J. Heat. Mass Transf. 42 (1999) 2003–2013, https://doi.org/10.1016/S0017-9310(98)00294-4.
[55] Silmet High Performance Copper, Ten Coppere Tube: cu-DHP CW024A. http://www.silmet.com/wp-content/uploads/2018/12/Ten_ENG.pdf (accessed 15 November 2023).
[56] Wickeder Westfalenstahl, Werkstoffdatenblatt CopperPlus. https://www.wickeder-group.de/fileadmin/Data/Divisions/Wickeder_Group/Download/WDB_Copper_Plus_deutsch_2016-03.pdf (accessed 15 November 2023).
[57] T. Sakai, S. Yoshii, K. Kajimoto, H. Kobayashi, Y. Shinmoto, H. Ohta, Heat transfer enhancement observed in nucleate boling of alcohol aqueous solutions at very low concentration, in: Proc. 14th Int. Heat Transfer Conf, Washington, DC, USA, 2010. IHTC14-22737.
[58] D. Gorenflo, E. Baumhögger, G. Herres, S. Kotthoff, Prediction methods for pool boiling heat transfer: a state-of-the-art review, Int. J. Refriger. 43 (2014) 203–226, https://doi.org/10.1016/j.ijrefrig.2013.12.012.
[59] S.A. Alavi Fazel, M. Jamialahmadi, A.A. Safekordi, Experimental investigation in pool boiling heat transfer of pure/binary mixtures and heat transfer correlations, Iran. J. Chem. Chemical Eng. (IJCCE) 27 (2008), https://doi.org/10.30492/ijcce.2008.6979.
[60] Y. Koizumi, M. Monde, N. Nagai, M. Shoji, Y. Takata (Eds.), Boiling: Research and Advances, Elsevier, 2017.
[61] J. Straub, A. Weinzierl, M. Zell, Thermokapillare grenzflächenkonvektion an gasblasen in einem temperaturgradientenfeld, Wärme Stoffübertr. 25 (1990) 281–288, https://doi.org/10.1007/BF01780740.
[62] D. Jung, K. Song, K. Ahn, J. Kim, Nucleate boiling heat transfer coefficients of mixtures containing HFC32, HFC125, and HFC134a, Int. J. Refriger. 26 (2003) 764–771, https://doi.org/10.1016/S0140-7007(03)00066-5.
[63] T. Inoue, M. Monde, Y. Teruya, Pool boiling heat transfer in binary mixtures of ammonia/water, Int. J. Heat. Mass Transf. 45 (2002) 4409–4415, https://doi.org/10.1016/S0017-9310(02)00153-9.
[64] F. Táboas, M. Vallès, M. Bourouis, A. Coronas, Pool boiling of ammonia/water and its pure components: comparison of experimental data in the literature with the predictions of standard correlations, Int. J. Refriger. 30 (2007) 778–788, https://doi.org/10.1016/j.ijrefrig.2006.12.009.